Cape Peninsula
University of Technology

Channel performance estimation for massive multiple input multiple output.

by

Randall Allister Press

Thesis submitted in fulfilment of the requirements for the degree

Master of Engineering: Electrical Engineering

in the Faculty of Engineering and the Built Environment

at the Cape Peninsula University of Technology

Supervisor: Dr. Vipin Balyan
Co-supervisor: Dr. Oluwaseyi P. Babalola

Bellville
March 2023

DECLARATION

I, Randall Allister Press, declare that the contents of this thesis represent my own unaided work, and that the thesis has not previously been submitted for academic examination towards any qualification. Furthermore, it represents my own opinions and not necessarily those of the Cape Peninsula University of Technology.

Signed  **Date 14 March 2023**

ABSTRACT

Global demand for connectivity has risen exponentially in the 4th industrial revolution. The 4th generation (4G) networks experienced difficulties meeting high demands of media centric communication. Due to spectrum limitation, the orthogonal resources were reaching their limits to satisfy user requirements. Demand has driven the need for 5th generation (5G) communication to provide spectral efficient, low latency, dense network communication. Investigation into non-orthogonal multiple access (NOMA) has been proposed over orthogonal multiple access (OMA) schemes. These include power domain NOMA and code domain NOMA. These schemes are capable of overloading resource elements with multiple users. These techniques show promise in addressing spectral efficiency, low latency, and dense network demands. Thus, a review of literature discusses the need for multiple user access and highlights the earlier techniques. Analysis shows that the SCMA codebook and decoders are effective at providing improved spectral efficiency while delivering a good bit error rate performance. This research aims to design an optimal sparse code multiple access (SCMA) codebook to improve bit error and spectral efficiency of multiple access uplink communication system. An SCMA codebook design is implemented on the uplink of communication system, where a maximum likelihood decoder is implemented at the receiver. The 16-APSK and 16-QAM constellations are used to design the SCMA codebooks, while optimization of the minimum Euclidean distance between neighbouring points is implemented to assist the decoder.

ACKNOWLEDGEMENTS

I wish to thank:

- God, for the gift of life and for surrounding me with beautiful people that always believed in me when I did not.
- My wife for being the rock when needed it the most.
- My parents for the support and making all this possible.
- Dr. Vipin, who never gave up on me when I did. A man who is wise and a great mentor.
- Dr. Babalola for his kindness and wisdom. Who provided perspective on complex information.
- The financial assistance of the National Research Foundation towards this research is acknowledged. Opinions expressed in this thesis and the conclusions arrived at, are those of the author, and are not necessarily to be attributed to the National Research Foundation.

DEDICATION

I dedicate this to my wife, and my daughter, who was able to make me smile in times of doubt. I would like to make special dedication to my parents, who prayed and fought to get me through a rough time following Covid.

TABLE OF CONTENTS

GLOSSARY

1G	First Generation
2G	Second Generation
3G	Third Generation
3G	Third Generation
3GPP	Third Generation Partnership Project
4G	Fourth Generation
5G	Fifth Generation
5G-NR	Fifth-generation New Radio
AMPS	Advanced Mobile Phone Services
AWGN	Additive White Gaussian Noise
BER	Bit Error Rate
CDMA	Code Division Multiple Access
CPS	Cyber-Physical Systems
EDGE	Enhanced Data rates for Global Evolution
eMBB	Extreme Mobile Broadband
FBMC	Filter-Bank Based Multi-Carrier
FDD	Frequency Division Duplex
FDMA	Frequency Division Multiple Access
FM	Frequency Modulation
FM	Frequency Modulation
GAM	Golden Angle Modulation
GPRS	General Packet Radio Services
GSM	Global System for Mobile communications
HSUPA	High-Speed Uplink Packet Access
ICT	Information and Communications Technology
IDMA	Interleave Division Multiple Access
IoT	Internet of Things
LDS	Low-Density Spreading
LTE	Long Term Evolution
LTE-A	
M2M	Machine-To-Machine
MAI	Multiple access interference
MBB	Mobile Broadband
MED	Minimum Euclidean Distance
MIMO	Multiple-Input Multiple-Output
ML	Maximum Likelihood
mMTC	Massive Machine Type Communication
MPA	Message Passing Algorithm
MUD	Multiple-User Detection
NFV	Network Function Virtualisation
NMT	Nordic Mobile Telephone

NOMA	Non-Orthogonal Multiple Access
OFDM	Orthogonal Frequency Division Modulation
OFDMA	Orthogonal Frequency Division Multiple Access
PAPR	Peak-To-Average Power
PLC	Programmable Logic Controllers
PS	Packet-Switched
PS	Packet Switch
QAM	Quadrature Amplitude Modulation
RE	Resource Element
SCMA	Sparse Code Multiple Access
SDN	Software Defined Networking
SIC	Successive Interference Cancellation
SMS	Short Messaging Service
SNR	Signal-To-Noise Ratio
TACS	Total Access Communications System
TCM	Trellis-Coded Modulation
TDMA	Time Division Multiple Access
UE	User Element
UFMC	Universal Filtered Multi-Carrier
uMTC	Ultra-Reliable Machine-Type Communication
URLLC	ultra-reliable, and low latency communication
WCDMA	Wideband Code Division Multiple Access

Chapter 1 Introduction

1.1 Research Motivation

Multiple access techniques for fifth-generations (5G) networks are at the forefront of the challenges of wireless networks and future technology. The standard of using orthogonal resources has seen a shift due to new technologies, such as the Internet of Things (IoT), massive machine type communication (mMTC), ultra-reliable, and ultra low latency communication (URLLC). The emerging technologies require the ability to serve an enormous number of connections, with the Third Generation Partnership Project (3GPP) setting diverse requirements arising from identified problem areas, such as latency and throughput (Vaezi et al., 2018). The research into non-orthogonal multiple access techniques, which is discussed in detail (Dai et al., 2015; Dai et al., 2018; Aldababsa et al., 2018) proposed solutions to the problem of the massive connectivity requirements of 5G.

1.2 Problem Statement

The original SCMA scheme proposed using multi-dimensional constellation, focuses on an ideal Euclidean distance (Taherzadeh et al., 2014). In (Liu et al., 2018), an optimized SCMA codebook design for uplink transmission was introduced to increase the minimum Euclidean distance (MED) by dividing a 16-point QAM constellation into several subsets. The division resulted in a noticeable improvement in bit-error rate (BER) and capacity performance compared to the scheme in Taherzadeh et al., 2014. Authors in (Wang et al., 2019) considered maximizing the MED as an essential design parameter for SCMA codebook design.

In (Mheich et al., 2019), a golden angle modulation (GAM) was proposed to obtain enhanced SCMA codebooks with a lowered peak-to-average power ratio (PAPR). Two codebook designs were presented such that each had independent optimisation parameters. The optimization parameters increased the normalised MED and decreased the PAPR. The authors considered a practical implementation with OFDM multicarrier techniques. The codebook design reports a PAPR lower than (Liu et al., 2018), with an improved BER.

A computer-aided algorithm was used to generate the SCMA codebooks in (Tabra & Sabbar, 2019). The method focused on maximizing MED using trellis-coded modulation (TCM). This scheme yielded an increase in MED by a factor of 3.2% and 2.3% compared to the literature in

(Liu et al., 2018). Thus, resulting to a marginal improvement in bit-error rate (BER) performance at low signal-to-noise ratio (SNR).

The lattice theory-based codebook design in (Zhang & Member, 2019), finds power-saving mother constellation with diverse power variations between constellation points. Lattice theory is used to ensure that a constellation has a small energy, while spherical capping is used to maximize the Euclidean distance of the constellation points. By combining these two techniques, it is possible to design a constellation with a constant minimum Euclidean distance (MED) and a low average energy. This is important for ensuring the reliability of communication systems that use QAM or APSK constellations. Lattice theory provides a mathematical framework for designing constellations with small energy, while spherical capping is a geometric technique that is used to maximize the distance between constellation points. Together, these techniques can be used to design constellations that are optimized for reliable communication. The proposed design improved BER performance, especially at high SNR though it does increase multiple-user detection (MUD) complexity. Nevertheless, expanding the codebook size significantly reduces the BER performance compared to the overload factor. Moreover, the improved power saving is a tradeoff of the overall BER performance as compared to the proposed schemes in (Tabra & Sabbar, 2019; Liu et al., 2018; Wang et al., 2019).

SCMA schemes have the potential to surpass orthogonal multiple access by supporting overloaded systems, low latency grant-free, and robust communication. The code-domain non-orthogonal multiple access technique used by SCMA schemes invests in the optimal constellation design and multi-user detection techniques for improved system performance (Taherzadeh et al., 2014). However, a major research problem is to develop an effective signalling constellation and multi-user detection scheme to mitigate the inherent multiple access interference in the massive MIMO system. This will help to enhance the spectral efficiency and probability of error of the system.

1.3 Research Question

How can SCMA codebooks be optimally constructed using APSK and 16-QAM constellations to enhance the spectral efficiency and bit error rate performance of uplink transmission from multiple users while achieving a reduced complexity?

1.4 Aim and Objectives

1.4.1 Aim

The aim of this research is to design a near optimal SCMA codebook with the maximum likelihood decoder to improve the system performance of uplink transmission from multiple users.

1.4.2 Objectives

i. Perform comprehensive survey of SCMA Codebook design and suitable decoding schemes.
ii. Understand key models using simulation and propose methods to enhance existing SCMA codebook designs.
iii. Develop and simulate the proposed SCMA codebook design using MATLAB.
iv. Compare the BER performance of the proposed codebook designs with results from the literature using MATLAB.

1.5 Delineation of research

The study is limited to uplink communication with a maximum of six users and four REs. The system assumes ideal channel state information for simulations. Modulation and demodulation are not implemented; it is understood that these system blocks are ideal. The study focuses on the performance of the designed codebooks over a Rayleigh fading channel with additive white Gaussian noise (AWGN).

1.6 Significance of Research

The study explores using three well-established high-order constellations as the mother constellation of the SCMA codebook. The constellations consist of two rings such that each constellation is distinguished from another by the position of their constellation points. The maximum Euclidean distances of all the constellation points are obtained by calculating the optimum ring ratio between the inner and outer rings of the constellation.

Sub-constellation from partitioning the mother constellation produced an increased minimum Euclidean distance (MED). The increased MED mitigates user interference and lowers the decoding complexity resulting in an improved BER performance. The output of this research is important for real time digital communication since the increased MED mitigates user interference. More so, the constructed codebook helps to improve the BER performance of the

system with a reduced decoding complexity, making it applicable for real time implementations.

1.7 Expected outcomes

1.8 Thesis outline

Chapter 1: Brief overview of the communication system and existing problems. This is addressed as problem statement, research question and the aim and objectives of the research.

Chapter 2: Discusses and reviews literature on SCMA codebook and decoder design. This builds research and provides the necessary understanding to implement SCMA communication systems.

Chapter 3: Discusses a fundamental part to SCMA codebook design and discusses information theory that builds onto the concept of SCMA codebook design optimization.

Chapter 4: Discusses the methodology of SCMA codebook design and the uplink system model which is implemented in later chapters. Methodology discussed in this chapter is used throughout later chapters.

Chapter 5 Implements theory on the Conventional Star 16-QAM mother constellation. SCMA Codebook is designed and compared over varying channels and other proposed SCMA codebooks.

Chapter 6 Implements theory on the Dual Star 16-QAM mother constellation. A SCMA Codebook is designed and compared over varying channels and other proposed SCMA codebooks.

Chapter 7 Implements theory on the 4+16 APSK mother constellation. A SCMA Codebook is designed and compared over varying channels and other proposed SCMA codebooks.

Chapter 8 Concludes the simulation results and SCMA codebook designs providing an overview of numerical simulation results. Furthermore, future prospects are discussed with knowledge gained over the course of completing the SCMA codebook designs.

1.9 Summary

This research aims to design an optimal SCMA codebook to improve the BER uplink communication performance to the base station. The objective is to research existing schemes and develop and approach to improve the BER parameter within an overloaded communication system. The methodology involves implementing theory fundamental to the performance of communication.

Chapter 2 Literature Review

2.1 Introduction

A core feature of telecommunication is multiple access (MA), which requires an exponential technological evolution. This chapter discusses the relevant literature and the key factors that enables SCMA communication schemes. The enabling technology allows the resources of a mobile communication system to be overloaded. This is achieved by SCMA codebook designs (CB) and decoding algorithms that enable multiuser detection (MUD). Codebook design aims to optimize the system's uplink and downlink performance over several channels. The codebook designs affect system performances, such as the BER or peak-to-average power ratio (PAPR). This has led to many studies addressing certain performance parameters, such as interleaving to improve the minimum Euclidean distance between codewords (Cai et al., 2016; Mheich et al., 2019; Yan et al., 2017). In (Vidal-Beltrán & López-Bonilla, 2021), machine learning method was utilised to improve spectral efficiency. Nevertheless, the optimal codebook is yet to be designed.

Furthermore, multiuser detection has been utilised alongside codebook designs to enhance the performance of SCMA communication. The popular MUD algorithm employed in the literature is the message passing algorithm (MPA) (Ameur et al., 2019; Ghaffari et al., 2019; Liu & Yang, 2021). The MPA takes advantage of the sparsity characteristics of the designed codebooks to avoid saturation in the tanner graph. Though in the case of MUD, there exist algorithms that approach the maximum *a-posteriori* (MAP) detector performance, the practical implementation is unrealized now.

Table.2-1: Notations

x	Scalar
$\boldsymbol{x}$	Vector
$\boldsymbol{X}$	Matrix
$\boldsymbol{x}^T, \boldsymbol{X}^T$	Transpose of $\boldsymbol{x}$,$\mathbf{X}$
$\mathbb{B}$	Binary number set
$\mathbb{C}$	Complex number set
$\boldsymbol{x}_i$	i^{th} element of $\boldsymbol{x}$
$\text{diag}(\boldsymbol{x})$	Diagonal matrix of $\boldsymbol{x}$
$\arg\max\left[f(x)\right]$	Value of x that maximises $f(x)$
$\log(\boldsymbol{x})$	Natural logarithm of vector $\boldsymbol{x}$ elements
$\max_x f(x)$	Maximum value of function $f(x)$ for all possible values of x
$N \times M$	N rows and M columns matrix
$\boldsymbol{I}_N$	N × N identity matrix

2.1.1 SCMA Encoding and Codebook Design

The SCMA encoding model in (Nikopour & Baligh, 2013) focuses on the uplink communications of a synchronous SCMA system, where *J* users utilise *K* resource elements for data transmission to the base station (BTS). For SCMA, an encoder maps the user's data bits to a complex codeword given by:

$$\mathbf{m}_j = \mathbf{CB}_j\left(\mathbf{b}_j\right), \tag{2.1}$$

where $\mathbf{b}_j$ is the data bits of user *j*, $\mathbf{m}_j \in \mathbb{A}_j \subset \mathbb{C}^K$ is the selected codeword from a codebook $\mathbf{CB}_j$, and $\mathbb{A}_j$ is user *j*th set of codewords.

The SCMA encoder consists of layers where the number of layers equals the number of users, and each user has an assigned codebook. The terms 'user' and 'layer' are interchangeable and assume each user has one layer. The design of sparse codebooks determines the performance gain of SCMA, specifically how well the designs are. Each user's codebook has a unique sparsity pattern written as a $K \times M$ matrix, where *M* is the number of codewords or the columns of the user's codebook matrix. In the CB matrix for each user, the column vector is sparse with d_v non-zero elements at resource elements (REs) that are fixed.

Most of the codebook designs are sub-optimal and based on multiple stages. A multi-dimensional codebook for user *j* is given by (Chaturvedi et al., 2021)

$$\mathrm{CB}_j = \mathbf{V}_j \Delta_j \mathbf{A}'_{MC}, \quad \text{for } j = 1, 2, \cdots, J \tag{2.2}$$

where $\mathbf{V}_j \in \mathbb{B}^{K \times d_\upsilon}$ is the binary mapping matrix, $\mathbf{A}'_{MC}$ is the multi-dimensional mother constellation, and Δ_j is the *j*th user's constellation operator. The selection of the mapping matrix for each user is such that each user's transmissions occur only over fixed REs.

The signature matrix (Sklar, 2001; Rappaport, 2002; Rice, 2009; Falconer, 2011; Wilson, 2012) in an SCMA system is an important tool for allowing multiple users to share the same resource element (RE) without causing interference. This is achieved by using sparse coding schemes, which allow the allocation of REs to users in a way that maximizes the number of users that can be supported on a given set of REs. In (Sklar, 2001; Rappaport, 2002; Rice, 2009; Falconer, 2011; Wilson, 2012), the signature matrix shows that the first two REs are allocated to users 1, 2, and 3, while the last two REs are allocated to users 2, 4, and 5. This allows multiple users to share the same RE without causing interference, as the allocation of REs is carefully designed to avoid collisions (Sklar, 2001; Rappaport, 2002; Rice, 2009; Falconer, 2011; Wilson, 2012).

In (Sklar, 2001; Rappaport, 2002; Rice, 2009; Falconer, 2011; Wilson, 2012), the signature matrix was used to create the mapping matrices. This indicates what sub-constellations each user is assigned to. Consider a (n,k) SCMA block, where n is the number of resource elements and k is the number of users. The authors in (Sklar, 2001; Rappaport, 2002; Rice, 2009; Falconer, 2011; Wilson, 2012) designed a codebook using n= 4 and k = 6 where a user 1 is assigned to the first two REs. The binary mapping matrix is obtained as:

$$\mathbf{V}_1 = \begin{bmatrix} 1 & 0 \\ 0 & 1 \\ 0 & 0 \\ 0 & 0 \end{bmatrix}, \mathbf{V}_2 = \begin{bmatrix} 1 & 0 \\ 0 & 0 \\ 0 & 1 \\ 0 & 0 \end{bmatrix}, \mathbf{V}_3 = \begin{bmatrix} 1 & 0 \\ 0 & 0 \\ 0 & 0 \\ 0 & 1 \end{bmatrix}, \mathbf{V}_4 = \begin{bmatrix} 0 & 0 \\ 1 & 0 \\ 0 & 1 \\ 0 & 0 \end{bmatrix}, \mathbf{V}_5 = \begin{bmatrix} 0 & 0 \\ 1 & 0 \\ 0 & 0 \\ 0 & 1 \end{bmatrix}, \mathbf{V}_6 = \begin{bmatrix} 0 & 0 \\ 0 & 0 \\ 1 & 0 \\ 0 & 1 \end{bmatrix}.$$

The signature matrix **F** shows the allocation of REs for each user,

$$\mathbf{F}=\left[f_1, f_2, \cdots, f_J\right],$$

where

$$f_j = \operatorname{diag}\left(\mathbf{V}_j \mathbf{V}_j^T\right).$$

The denotation for active transmission of user *j* using the *k*th RE is given by

$$\mathbf{F}_{jk} = 1.$$

The following example shows the signature matrix of a (4,6) SCMA block, consisting of 4 REs and 6 users, where $K = 4$ and $J = 6$.

$$\mathbf{F}_{4\times 6} = \begin{bmatrix} 1 & 1 & 1 & 0 & 0 & 0 \\ 1 & 0 & 0 & 1 & 1 & 0 \\ 0 & 1 & 0 & 1 & 0 & 1 \\ 0 & 0 & 1 & 0 & 1 & 1 \end{bmatrix}. \quad \textbf{(2.3)}$$

The design of the mother constellation is an important step in SCMA communication (Rappaport, 2002). The mother constellation is a reference constellation that is used to generate the codebooks for each user. By carefully designing the mother constellation, it is possible to improve the performance of the SCMA system. This reduces multiuser interference and increases the shaping gain of the constellation. Once the mother constellation is designed, the codebooks for each user can be generated as discussed in (Rappaport, 2002). Operations such as unitary rotations, complex conjugates, phase rotations, dimensional permutations, and layer power offsets are applied to the mother constellation to obtain the codebooks. These operations are used to create the unique codebooks for each user, which are then used for encoding and transmitting the user's data. Overall, the design of mother constellation and the generation of codebooks are critical steps in SCMA communication (Rappaport, 2002).

The following example illustrates the design steps of a $J = 6$ and $K = 4$ SCMA codebook, where $J/K = 1.5$ is the overloading factor and $d_f = 3$ is the number of superimposed users on each RE.

Example 1:

Step 1: Starts with the design of a complex vector $\mathbf{\Lambda}_1$

$$\mathbf{\Lambda}_1 = \left\{ Y_m \left(1+i\right) \middle| Y_m = 2m-1-M, \;\; m = 1, \cdots, M \right\}$$
$$\text{For } M = 4, \; \mathbf{\Lambda}_1 = \left\{ -3\left(1+i\right), -1\left(1+i\right), 1\left(1+i\right), 3\left(1+i\right) \right\}$$

Step 2: For codeword's non-zero elements d_υ

$$\mathbf{\Lambda}_{d_\upsilon} = \mathbf{U}_{d_\upsilon} \mathbf{\Lambda}_1$$

where the phase rotation matrix is $\mathbf{U}_{d_\upsilon} = \text{diag}\left(\mathbf{1} e^{\theta_{d_\upsilon}} \right)$, the d_υ-dimensional vector consisting of only ones is $\mathbf{1}$, and $\theta_{d_\upsilon} = \frac{(d_\upsilon - 1)\pi}{d_\upsilon}$. The mother constellation for the above-mentioned is shown below:

$$\mathbf{\Lambda}_{MC} = \left[\mathbf{\Lambda}_1, \cdots, \mathbf{\Lambda}_{d_v} \right]^T$$
$$= \begin{bmatrix} \lambda_{11} & \lambda_{12} & \cdots & \lambda_{1M} \\ \lambda_{21} & \lambda_{22} & \cdots & \lambda_{2M} \\ \vdots & \vdots & \vdots & \vdots \\ \lambda_{d_v 1} & \lambda_{d_v 2} & \cdots & \lambda_{d_v M} \end{bmatrix}$$

Step 3: This step implements interleaving and reorders the mother constellation's even elements. The interleaving improves the performance of the codewords in a fading channel and reduces the mother constellation's PAPR.

For $d_\upsilon = 2$ and $M = 4$, this is the second row of the mother constellation $\mathbf{\Lambda}_2 = \left\{ \lambda_{21}, \lambda_{22}, \lambda_{23}, \lambda_{24} \right\}$ with the elements reordered, it becomes $\mathbf{\Lambda}_2^{'} = \left\{ \lambda_{22}, \lambda_{24}, \lambda_{21}, \lambda_{23} \right\}$

The completed mother constellation is $\mathbf{\Lambda}_{MC}^{'} = \left[\mathbf{\Lambda}_1, \mathbf{\Lambda}_2^{'}, \mathbf{\Lambda}_3 \right]^T$

Step 4: This step is the generation of the codebooks for all the users, where the phase rotation angle is:

$$\omega_u = \exp\left(\frac{i\pi u}{d_v d_f}\right), \quad \text{for } u = 0,1,\cdots,d_f - 1$$

The utilisation of Latin order takes the non-zero elements of the factor graph and assigns the phase rotation angle (ω_u) to those positions, where $\omega_0 = 1$, $\omega_1 = \exp\left(\frac{i\pi}{6}\right)$, $\omega_2 = \exp\left(\frac{i\pi}{3}\right)$ for $J = 6$, $M = 4$, $d_\upsilon = 2$, and $d_f = 3$. The phase rotation assignment of the signature matrix is

$$\mathbb{F} = \begin{bmatrix} \omega_0 & \omega_1 & \omega_2 & 0 & 0 & 0 \\ \omega_1 & 0 & 0 & \omega_2 & \omega_0 & 0 \\ 0 & \omega_2 & 0 & \omega_0 & 0 & \omega_1 \\ 0 & 0 & \omega_0 & 0 & \omega_1 & \omega_2 \end{bmatrix}$$

At this point, the codebooks for all the users can be generated using equation (2.2), where $\Delta_j = \text{diag}(\mathbf{w}_j)$.

2.1.2 Uplink communications of a symbol-synchronous SCMA

In a symbol-synchronous SCMA system, the uplink communications involve J users utilizing K resource elements to transmit data to the base station (BS). User j's codeword is $\mathbf{m}_j$, where $\mathbf{m}_j \in \mathbb{C}^{K\times 1}$ with cardinality $M = 2^b$ and b is the number of bits in a codeword. As before, this example is for a (4,6) SCMA system, where the codebook contains 4 codewords $(M = 4)$ and the mapping is over two binary bits.

The channel fading coefficient matrix for user *j* in the uplink SCMA is $\mathbf{h}_j = \left[h_{1j}, \cdots, h_{Kj}\right]^T$, where h_{kj} is the channel fading coefficient for user *j* at RE *k*. The codeword for user *j* is $\mathbf{m}_j = \left[C_{1,j}, \cdots, C_{K,j}\right]^T$, where $C_{k,j}$ is the element of the codeword transmitted on RE *k* by user *j*. The signal received by the base station is given (Chaturvedi et al., 2021).

$$\mathbf{y} = \sum_{j=1}^{J} \operatorname{diag}\left(\mathbf{h}_j\right)\mathbf{m}_j + \mathbf{n}, \tag{2.4}$$

where the noise vector is $\mathbf{n} \in \mathbb{C}^{K\times 1}$ consisting of complex Gaussian distribution elements modelled as $\mathcal{CN}\left[0, \sigma^2\right]$.

In the SCMA system, overlapping of non-zero values of d_f occurs over the resource elements, where the users transmit data on $d_\upsilon = K$ REs. A user set utilising the *k*th RE for data transmission is ξ_k and the resource element set on which active transmissions of user *j* occurs is ζ_j. The number of elements of ξ_k and ζ_j are d_f and d_υ, respectively. The signal received by RE *k* is given by (Chaturvedi et al., 2021)

$$y_k = \sum_{j\in\xi_k} h_{kj} C_{k,j}\left(\mathbf{m}_j\right) + n_k, \quad \text{for } k = 1, 2, \cdots, K. \tag{2.5}$$

The matrix given in equation (2.3) for a (4,6) SCMA system has an overload factor of users compared to Res, $\lambda = J/K = 1.5$. The rows and columns of the signature matrix $\mathbf{F}_{4\times 6}$ correspond to a RE and user, respectively. Each RE has several superimposing users equal to $d_f = 3$, and each column's non-zero value is $d_\upsilon = 2$. The signal received by RE *k* is given by (Chaturvedi et al., 2021)

$$y_k = h_{k1} C_{k,1}\left(\mathbf{m}_1\right) + h_{k2} C_{k,2}\left(\mathbf{m}_2\right) + h_{k3} C_{k,3}\left(\mathbf{m}_3\right) + n_k, \quad \text{for } k = 1, 2, \cdots, K. \tag{2.6}$$

The user set belonging to ξ_k has the codewords $\mathbf{m}_1, \mathbf{m}_2, \mathbf{m}_3$. The interfering user set on RE one is $\xi_1 = \{1, 2, 3\}$, and user 1's active transmission RE set is $\zeta_1 = \{1, 2\}$. In the same manner, the interfering user set on RE two is $\xi_2 = \{1, 4, 5\}$.

2.2 Decoding

Decoding is a procedure that extracts the signal of interest from the received noisy signal. The types of decoding fall into two categories; 1) hard decision decoding (HDD) and 2) soft decision decoding (SDD). The HDD decodes the received value as 1 or 0 based on a threshold value. The decoder performs decoding without knowing if the received value is close to or far from the threshold value. On the other hand, SDD utilises an estimated sequence and its reliability level. The estimation and detection of soft decoding is an iterative process that increases data extraction from the received signal.

2.2.1.1.1 Hard Decoding

In the hard decoding process, the received signal **y** passes through the thresholding step, where the evaluation of each $y_i \in \mathbf{y}$ occurs, shown in Figure 2.1. The evaluation is as follows, if $y_i > 0$, then $d_i = 0$; else, if $y_i < 0$, then $d_i = 1$, where $d_i \in \mathbf{d}$.

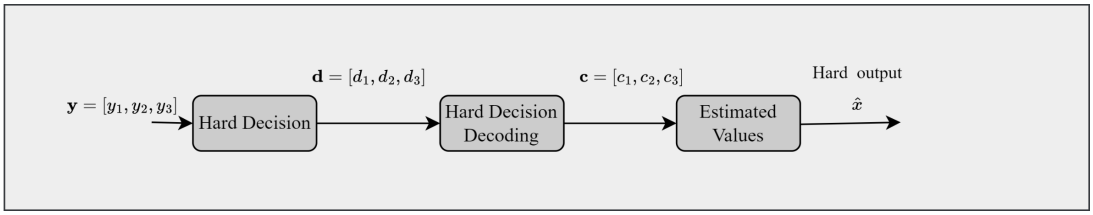

Figure 2.1: Process of Hard Decoding

For example, let $\mathbf{y} = [0.02, -2, -0.4]$ represent the received vector and the hard threshold value of 0. Thus for $y_1 = 0.02$, the decoder decides $d_1 = 0$, $y_2 = -2$, so the decoder decides $d_2 = 1$, and $y_3 = -0.4$, so the decoder decides $d_3 = 1$. The decision confidence of the received signals y_1, y_2, and y_3 are low, high, and not as high as y_2 but higher than y_1, respectively. Due to the various levels of confidence in the estimated sequence **d,** whether they are correct is in question. On completion of the **d**, the determination of the Hamming distance for all codeword **d** and **c** possibilities occurs. When implementing the repetition code, $\mathbf{c} = [x, x, x]$ has two possibilities, either $[000]$ or $[111]$. The next step is evaluating **d** and assigning **c** based on the Hamming distance. Table 2-2 is the hard decoding table showing the values of **d**, **c,** and $\hat{x}$ and the grouping of column one's values is closer to $c = [000]$ and $c = [111]$, respectively. As the name suggests, repetition coding transmits the same data repeatedly; however, utilising information is inefficient.

Table 2-2: Hard Decoding Table

d	c	$\hat{x}$
000	000	0
001	000	0
010	000	0
100	000	0
011	111	1
101	111	1
110	111	1
111	111	1

2.2.1.1.2 Soft Decoding

Soft decoding is a method of error correction used in digital communication systems that allows the decoder to make probabilistic decisions about the transmitted data based on the relative likelihoods of different possible values (Fossorier et al., 1999). One way to implement soft decoding is using log-likelihood ratios (LLRs), which are a measure of the relative likelihood of different possible values of a transmitted bit based on the received message (Hagenauer, 1988). LLRs can be calculated using a variety of techniques, such as the additive white Gaussian noise (AWGN) channel model (Cover & Thomas, 1991) or the sum-product algorithm (Kschischang et al., 2001). The decoder can then use the LLRs as input to make probabilistic decisions about the transmitted data, improving the accuracy of the decoding process in situations where the received message is noisy or the error rate is high (Chandrasetty & Aziz, 2009). In this introduction, we will provide an overview of the principles and benefits of soft decoding with LLRs, as well as some of the techniques and algorithms used to implement this approach (Zhang & Kschischang, 2017).

Log-likelihood ratios (LLRs) $[L_1, L_2, L_3]$ form the output vector for binary variables, where these real numbers indicate the reliability that $x_i = 0$. Bayes' rule computes the reliability of the received value to improve detection, given by equations (2.7) and (2.8).

$$P(c_1 = 0 | y_1) = \frac{f(y_1 | c_1 = 0) P(c_1 = 0)}{f(y_1)} \quad \textbf{(2.7)}$$

$$P(c_1 = 1 | y_1) = \frac{f(y_1 | c_1 = 1) P(c_1 = 1)}{f(y_1)} \quad \textbf{(2.8)}$$

Table 2-3: Bayes' Rule Notations

$P(c_1 = 0 \mid y_1)$	The probability that $c_1 = 0$ given y_1
$P(c_1 = 1 \mid y_1)$	The probability that $c_1 = 1$ given y_1
$P(c_1 = 0)$ and $P(c_1 = 1)$	The transmit bit's previous probabilities
$f(y_1 \mid c_1 = 0)$	The conditional distribution of y_1 given $c_1 = 0$
$f(y_1 \mid c_1 = 1)$	The conditional distribution of y_1 given $c_1 = 1$
$f(y_1)$	The probability distribution function of y_1

The equal probability of transmission for a BPSK modulated signal gives $P(c_1 = 0) = P(c_1 = 1) = 1/2$ and utilizing equations (2.7) and (2.8) yield:

$$\frac{P(c_1 = 0 \mid y_1)}{P(c_1 = 1 \mid y_1)} = \frac{f(y_1 \mid c_1 = 0)}{f(y_1 \mid c_1 = 1)}. \tag{2.9}$$

For $c_1 = 0$ and $c_1 = 1$, $y_1 = 1 + \mathcal{N}(0, \sigma^2)$ and $y_1 = -1 + \mathcal{N}(0, \sigma^2)$ respectively. Thus, equation (2.9) becomes the LLR shown by equation (2.10) based on y_1.

$$\begin{aligned} \frac{P(c_1 = 0 \mid y_1)}{P(c_1 = 1 \mid y_1)} &= \frac{\frac{1}{\sigma\sqrt{2\pi}} \exp\left(-(y_1 - 1)^2 / 2\sigma^2\right)}{\frac{1}{\sigma\sqrt{2\pi}} \exp\left(-(y_1 + 1)^2 / 2\sigma^2\right)}. \\ &= \exp\left(\frac{2y_1}{\sigma^2}\right) \end{aligned} \tag{2.10}$$

Thus, utilizing the received bits y_1, y_2, y_3, the repetition coding improves the transmit bit's reliability by repeating each bit thrice. The transmit bit's LLR is given by

$$L_1 = \log \frac{P(c_1 = 0 \mid y_1, y_2, y_3)}{P(c_1 = 1 \mid y_1, y_2, y_3)}. \tag{2.11}$$

Using Bayes' rule again results in equations (2.12) and (2.13)

$$P\left(c_1=0\middle|y_1,y_2,y_3\right)=\frac{f\left(y_1,y_2,y_3\middle|c_1=0\right)P\left(c_1=0\right)}{f\left(y_1,y_2,y_3\right)}, \tag{2.12}$$

$$P\left(c_1=1\middle|y_1,y_2,y_3\right)=\frac{f\left(y_1,y_2,y_3\middle|c_1=1\right)P\left(c_1=1\right)}{f\left(y_1,y_2,y_3\right)}. \tag{2.13}$$

The simplified form of equation (2.11) is given by

$$\begin{aligned} L_1 &= \log\frac{f\left(y_1,y_2,y_3\middle|c_1=0\right)}{f\left(y_1,y_2,y_3\middle|c_1=1\right)} \\ &= \log\left(\frac{\exp\frac{-(y_1-1)^2}{2\sigma^2}\exp\frac{-(y_2-1)^2}{2\sigma^2}\exp\frac{-(y_3-1)^2}{2\sigma^2}}{\exp\frac{-(y_1+1)^2}{2\sigma^2}\exp\frac{-(y_2+1)^2}{2\sigma^2}\exp\frac{-(y_3+1)^2}{2\sigma^2}}\right) \\ &= \frac{y_1+y_2+y_3}{2\sigma^2}. \end{aligned} \tag{2.14}$$

Using the same process L_2 and L_3 can be calculated, where $\frac{1}{2\sigma^2}$ is omitted because it is a constant. Thus, if $y_1+y_2+y_3>0$, the decoder decides $\hat{\mathbf{c}}=[000]$ or else $\hat{\mathbf{c}}=[111]$. Soft decoding efficiently utilises the received values, where estimation and a certain confidence level occur.

2.2.2 MAP Detection

The optimal detector minimizes the transmitted bit sequence's (**x**) error probability $\left(P(e)\right)$. This reduces the transmitted $\left(\mathbf{x}\right)$ and estimated $\left(\hat{\mathbf{x}}\right)$ bit's mismatch given by equation (2.15).

$$\min P(e)=\min P\left(\mathbf{x}\neq\hat{\mathbf{x}}\right). \tag{2.15}$$

The channel coefficient **H** and all **y**'s are given by the probability of error equation because they are directly related to the transmission of information through a communication channel (Proakis & Salehi, 2007). When a signal is transmitted through a channel, it is subject to various forms of noise and interference, which can affect the accuracy of the transmitted information. The probability of error equation is a mathematical expression that describes the likelihood of errors occurring during the transmission of a signal. Furthermore,

$$P(e) = \int P(e|\mathbf{y}) f(\mathbf{y}) d\mathbf{y} . \quad \textbf{(2.16)}$$

$P(e|\mathbf{y})$ is the error probability given **y** and $f(\mathbf{y})$ is the probability density function (pdf) of **y**. One of the key factors that determines the probability of error is the channel coefficient **H**, which is a measure of the strength and quality of the communication channel (Haykin, 2008). The value of **H** is determined by the characteristics of the channel, such as its bandwidth, signal-to-noise ratio, and the type of modulation used. A higher value of **H** indicates a better-quality channel with a lower probability of error, while a lower value of **H** indicates a poorer quality channel with a higher probability of error. Equation (2.16) shows the proportionality of $P(e)$ and $P(e|\mathbf{y})$, and the signal of interest is **x**; the error probability is given by equation (2.17)

$$P(e|\mathbf{y}) = 1 - P(\mathbf{x}|\mathbf{y}). \quad \textbf{(2.17)}$$

The probability of **x** given **y** is $P(\mathbf{x}|\mathbf{y})$. Maximum a-posteriori (MAP) detection minimizes the probability of error $P(e)$ by maximizing the probability of **x** given **y**, $P(\mathbf{x}|\mathbf{y})$. Applying Bayes' rule again gives equation (2.18).

$$P(\mathbf{x}|\mathbf{y}) = \frac{f(\mathbf{y}|\mathbf{x}) P(\mathbf{x})}{f(\mathbf{y})}. \quad \textbf{(2.18)}$$

The conditional pdf of **y** is $f(\mathbf{y}|\mathbf{x})$ given **x**, and the pdf of **y** is $f(\mathbf{y})$. The pdf of **y** is constant for all **x**'s possible values. Assuming previous probabilities are the same for varying x values; this yields equation (2.19)

$$P(\mathbf{x}|\mathbf{y}) \propto f(\mathbf{y}|\mathbf{x}). \quad \textbf{(2.19)}$$

The maximum likelihood (ML) detection scheme reduces the probability of error by choosing **x,** resulting in the maximization of the function $f(\mathbf{y}|\mathbf{x})$. If the previous probabilities are equal, then the ML and MAP detection schemes are the same.

2.2.2.1.1 MAP Detection in SCMA:

Given **y** and the channel matrix **H**, the multiuser codeword detected at the receiver for the SCMA's decoder, is shown by equation (2.20)

$$\hat{\mathbf{X}} = \underset{\mathbf{m}_j \in \mathbb{A}_j, \forall j}{\arg\max}\ p\left(\mathbf{X}|\mathbf{y}\right), \tag{2.20}$$

where the transmitted codeword of user j is $\mathbf{m}_j$ and the codeword set allocated to user j (user j's codebook) is $\mathbb{A}_j$. The maximization of the a-posteriori probability mass function (PMF) enables the estimation of each user's transmitted codeword, calculated using equation (2.20). The expression takes the marginal with respect to the joint a-posteriori PMF. Thus, the aim is to detect each user's transmitted codeword one by one.

2.2.3 Factor Graphs

Nodes and edges make up a graph's composition, where connected nodes indicate a relationship between the nodes. Graphs are visual aid representations used for problem modelling, where a bipartite graph models problems, specifically for communication and signal processing systems. Figure 2.2 is a bipartite graph composed of node sets A and B.

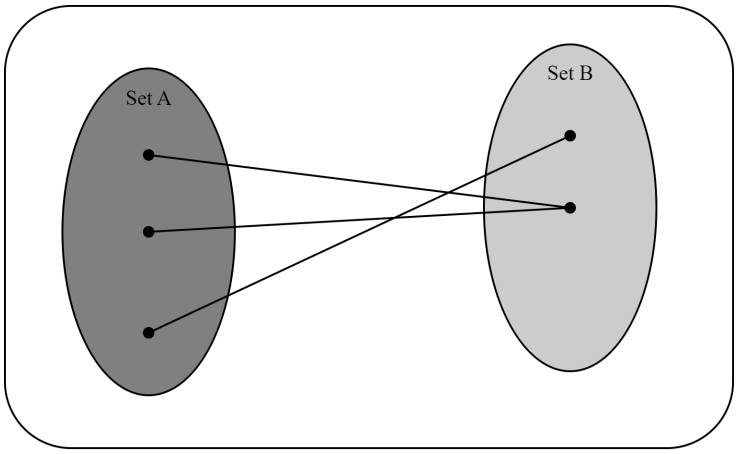

Figure 2.2: Bipartite Graph

A factor graph is a version of a bipartite graph composed of two groups of nodes called variable nodes (VNs) and function nodes (FNs), where the connection between two nodes occurs when a specific variable is that function's argument. A factor graph represents a global function in a less complex local function and utilizes a sum-product algorithm (SPA) to aid the marginal distribution computation.

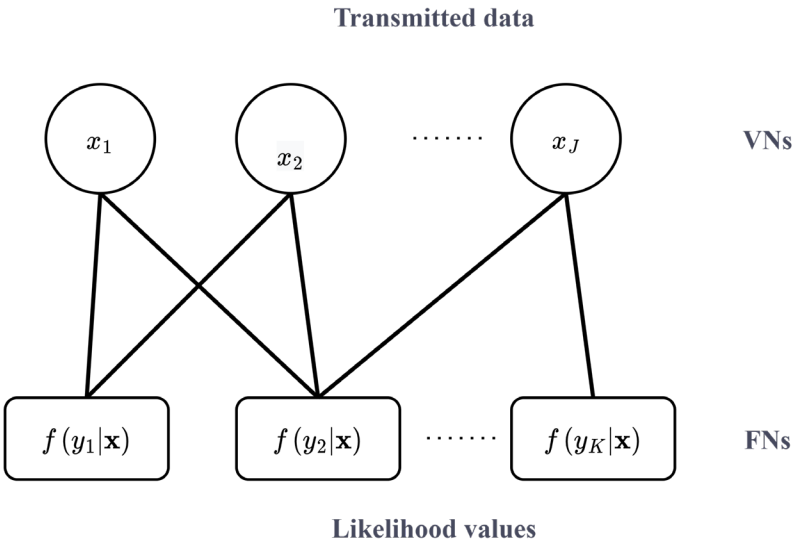

Figure 2.3: Communication Channel's Factor Graph

In the communication channel, the transmit vector is $\mathbf{x}=\left[x_1,x_2,\cdots,x_j,\cdots,x_J\right]$, and the received vector is $\mathbf{y}=\left[y_1,y_2,\cdots,y_k,\cdots,y_K\right]$ with independent noise components, resulting in equation (2.21)

$$f\left(\mathbf{x}|\mathbf{y}\right)=\prod_{k=1}^{K}f\left(y_k|\mathbf{x}\right). \tag{2.21}$$

The received symbol y_k depends on the vector **x**'s elements, i.e., x_1,x_2,x_j. Thus, the edge connections of the factor graph are between the FNs and VNs corresponding to $f\left(y_k|x_1,x_2,x_j\right)$ and x_1,x_2,x_j, respectively. Figure 2.3 shows the VNs and FNs indicating transmit points and likelihood functions $f\left(y_k|\mathbf{x}\right)$, respectively.

2.2.4 Message Passing Algorithm

A message passing algorithm (MPA) passes messages between nodes of a factor graph and reaches a decision based on the belief or confidence in the passed messages. Figure 2.4 shows an example of an MPA using students who stand in a line, where each student performs a head count and passes this number to the other students. However, the number of students to which each one can communicate is only two, the student in the front and back of the current student. So, the MPA approach is for each student to add 1 to the received count and then pass it along to the next student. The algorithm counter commences at 1 and from both ends of the line, incrementing by 1 as it progresses through each student.

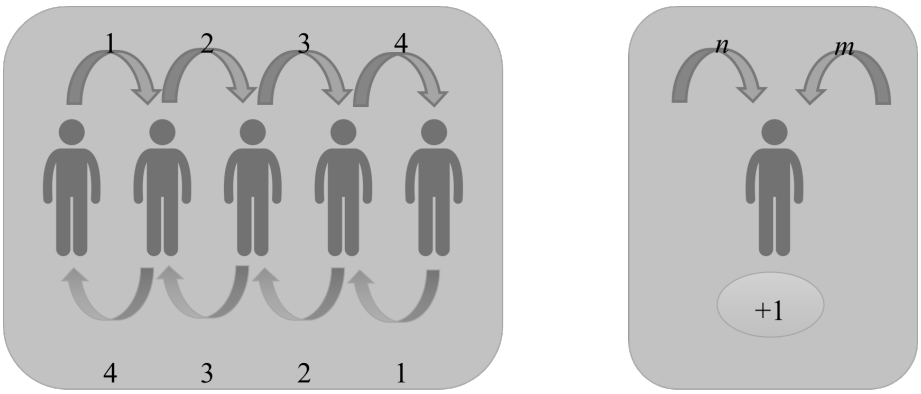

(a) (b)

Figure 2.4: MPA Student Example (Kschischang et al., 2001)

Thus, the total number of students is $n+m+1$, where *n* and *m* are the counts from the left and right side respectively. This example shows that a graph can model problems like this, where a student and connecting edge represent a node and communication link, respectively.

2.2.5 Message Passing Between Nodes

This section focuses on the factor graph and the message passing between Fixed nodes (FNs) and variable nodes (VNs). using a Sum-product algorithm (SPA). In an SCMA system, the total number of VNs and FNs equals the number of users/layers and REs, respectively. Suppose he transmitted and received bits are $\mathbf{c}=[c_1,c_2,\cdots,c_N]$ and $\mathbf{y}=[y_1,y_2,\cdots,y_N]$, respectively, then the *a posteriori* probability (APP) computation of bit c_i. i.e., $P(c_i=0|\mathbf{y})$ is the objective. Bayes' rule converts the APP with respect to c_i to likelihood ratios, as shown below

$$\frac{P(c_i=0|\mathbf{y})}{P(c_i=1|\mathbf{y})}=\frac{f(\mathbf{y}|c_i=0)}{f(\mathbf{y}|c_i=1)}.$$

The above ratio becomes the Log-likelihood ratio (LLR) of c_i by taking the natural logarithm given below

$$\mathrm{LLR}(c_i)=\log\left(\frac{f(\mathbf{y}|c_i=0)}{f(\mathbf{y}|c_i=1)}\right).$$

Thus, if $\mathrm{LLR}(c_i)<0$, then the decoded $c_i=1$, otherwise $c_i=0$.

If a factor graph contains closed loops, the message passing is iterative when using SPA. Each iterative step involves passing belief messages from VNs to FNs, and passing messages from FNs to VN.

Step 1: Forward passing:

This example uses a VN denoted by j_1 with connections to three FNs denoted by k_1, k_2, k_3, as illustrated in Figure 2.5.

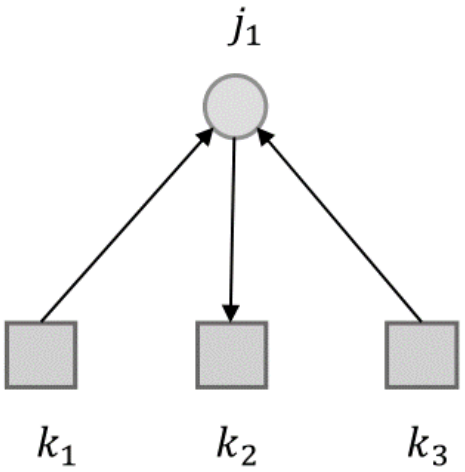

Figure 2.5: VN to FN Messaging Passing (Kschischang et al., 2001)

For VN j_1 to pass a message to FN k_2, it first multiplies the neighbouring node's received messages k_1 and k_3 then transfers the output to FN k_2, where the belief message between VN j_1 and FN k_2 (from VN to FN) is $n_{j_1 \to k_2}$

$$n_{j_1 \to k_2} = n_{k_1 \to j_1} \quad n_{k_3 \to j_1}.$$

The VN's outgoing message can be in either form, APP ratio $\left(P\left(c_i = 0 \middle| \mathbf{y}\right)\right)$ or likelihood ratio.

Step 2: Backward passing:

This step is the belief message passing in the opposite direction, from an FN to a VN. For this example, regard an FN denoted by k_1 with connections to three VNs denoted by j_1, j_2, j_3, as illustrated in Figure 2.6.

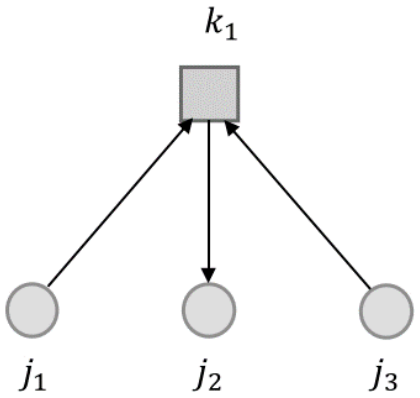

Figure 2.6: FN to VN Message Passing (Kschischang et al., 2001)

For FN k_1 to pass a message to VN j_2, it first collects the neighbouring node's received messages and multiplies them with FN k_1's associated local function $\left(f_{k_1}(j_1, j_2, j_3)\right)$; then, the SPA marginalizes the resulting function. The marginalized transmit message for VN j_2 is given below

$$n_{k_1 \to j_2} = \sum_{\sim j_2} \left(f_{k_1}(j_1, j_2, j_3) \; n_{j_1 \to k_1} \quad n_{j_3 \to k_1} \right),$$

where FN k_1's local function is $f_{k_1}(j_1, j_2, j_3)$, the belief message between FN k_1 and VN j_2 (from FN to VN) is $n_{k_1 \to j_2}$. This way, the belief message passing between FN k_1 and the other VNs is similar.

As shown in steps 1 and 2, belief message passing between FNs and VNs is bidirectional $(\text{FN} \Leftrightarrow \text{VN})$. Exact computations of APPs are possible if the factor graph's message passing is statistically independent, as is the case for a cyclic factor graph where independent assumptions are only valid for initial iterations. Practical simulation results show the efficacy of an MPA for computing LLRs or APPs.

2.2.6 Sum-Product Algorithm

Suppose a factor graph composed of J variable and K function nodes. The sum-product algorithm (SPA) message starting point is from a leaf node. Each node has several connected edges d and waits for messages from $d-1$ edges. The messages from VN j to FN k and FN k to VN j are $n_{j\to k}$ and $n_{k\to j}$, respectively. The node sets connected to VN j and FN k are ζ_j and $R=\xi_k$, respectively. The information symbol transmission set from VN j is $\mathbb{A}_j$ and $a_j \in A_j$. The SPA follows the following procedure:

1) The message passed from FN k to VN j is given by equation (2.22)

$$n_{k\to j}\left(a_j\right)=\sum_{\sim a_j}\left(\psi\left(R\right)\prod_{r\in R\setminus\{j\}} n_{r\to k(a_r)}\right) \quad \text{for } a_j \in A_j\text{,} \tag{2.22}$$

where FN k's associated likelihood function is $\psi\left(R\right)$ and all R's VNs except VN j is $r \in R\setminus\{j\}$. Also, the message from VN r to FN k with respect to the symbol a_r is $n_{r\to k}\left(a_r\right)$.

2) The message passed from VN j to FN k is given as

$$n_{j\to k}\left(a_j\right)=\prod_{d\in\zeta_j\setminus\{k\}} n_{d\to j(a_j)} \quad \text{for } a_j \in A_j\text{,} \tag{2.23}$$

where $d \in \zeta_j \setminus\{k\}$ is the FNs in ζ_j except FN k. Equation (2.24) is the normalized message confirming that the probability summation equals 1.

$$n_{j\to k}\left(a_j\right)=\frac{\prod_{d\in\zeta_j\setminus\{k\}} n_{d\to j}\left(a_j\right)}{\sum_{a_j}\prod_{d\in\zeta_j\setminus\{k\}} n_{d\to j}\left(a_j\right)} \quad \text{for } a_j \in A_j\text{.} \tag{2.24}$$

The sum-product algorithm is so named because it utilizes sum and product operations.

2.2.7 SCMA Decoding

This section is the design process of an SCMA factor graph using the signature matrix, and each user's transmitted symbol detection using SPA. The factor graph consists of VNs and FNs, which denote the users and resources in an SCMA system, respectively. The $\mathbf{F}_{4\times6}$ signature matrix (2.3) has d_v and d_f number of ones in each column and row, respectively. The rows and columns of the signature matrix correspond to a RE and user, respectively. In the first column of the signature matrix $\mathbf{F}_{4\times6}$, the first and second rows have non-zero values, meaning user 1 uses the first and second resource elements for data transmission. Thus, edges exist between VN j_1 and FN k_1 and k_2, respectively. In the second row of the signature matrix, the first, fourth, and fifth columns have non-zero values, meaning users 1, 4, and 5s data overlap on the second resource element. Thus, edges exist between FN k_2 and VN j_1, and VN j_4, and VN j_5, respectively. Figure 2.7 is the factor graph corresponding to the $\mathbf{F}_{4\times6}$ signature matrix.

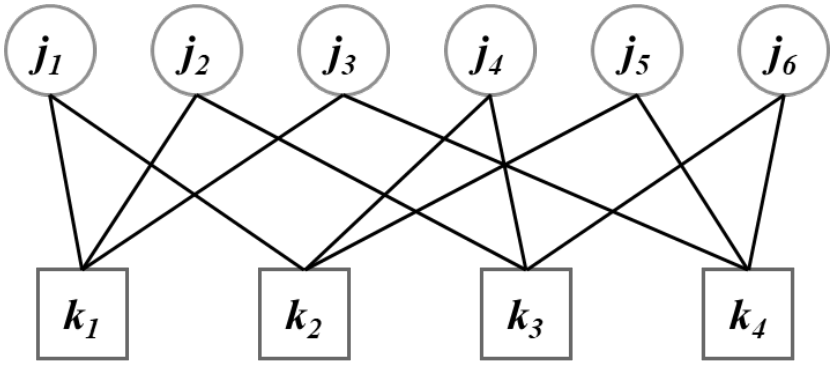

Figure 2.7 Factor Graph of 4x6 Signature Matrix (Kschischang et al., 2001)

2.2.7.1.1 SCMA Decoding using SPA

For the SCMA decoding, the objective is to detect each user's transmitted message by processing equation (2.25) using SPA. The SCMA system represented by the factor graph in Figure 2.7 employs the SPA to pass messages over the factor graph in both directions. This implies that messages are passed from VN to FN and vice versa. The message passing for this factor graph occurs for several iterations, only terminating when the number of iterations reaches a specified criterion. The following steps describe the SPA process for computing.

$$\hat{\mathbf{m}}_j = \arg\max_{\mathbf{m}_j \in \mathbb{A}_j} \sum_{\sim \mathbf{m}_j} \left(P(\mathbf{X}) \prod_{k=1}^{K} f\left(y_k \middle| \mathbf{X}\right) \right) \quad \text{for } j = 1, \cdots, J \,. \tag{2.25}$$

Step 1: Initialisation

This step computes the likelihood ratio at each FN, assuming the receiver knows **y** and **H**, the received vector, and the channel coefficient matrix. Consider a FN l with three users' corresponding data set $\xi_l = \{\upsilon_1, \upsilon_2, \upsilon_3\}$ to superimpose on an RE. Thus, FN l's likelihood function becomes $f\left(y_1 \middle| \mathbf{m}_1, \mathbf{m}_2, \mathbf{m}_3, N_0\right)$, where the user set of ξ_l have transmitted codewords $\mathbf{m}_1, \mathbf{m}_2, \mathbf{m}_3$. Assume $\mathbb{A}_\upsilon$ is the codeword set allocated to user υ. Equation (2.26) is the likelihood function of FN l

$$f\left(y_l \middle| \mathbf{m}_1, \mathbf{m}_2, \mathbf{m}_3, N_0\right) = \exp\left(\frac{-1}{N_0} \left\| y_l - \begin{pmatrix} h_{l1} C_{l,1}\left(\mathbf{m}_1\right) + \\ h_{l2} C_{l,2}\left(\mathbf{m}_2\right) + \\ h_{l3} C_{l,3}\left(\mathbf{m}_3\right) \end{pmatrix} \right\|^2 \right), \quad \text{for } \mathbf{m}_1 \in \mathbb{A}_1, \mathbf{m}_2 \in \mathbb{A}_2, \mathbf{m}_3 \in \mathbb{A}_3 \tag{2.26}$$

$C_{l,\upsilon}\left(\mathbf{m}_\upsilon\right)$ is the user υ's codeword element when transmitting $\mathbf{m}_\upsilon$ codeword over resource element l. The function $f\left(y_1 \middle| \mathbf{m}_1, \mathbf{m}_2, \mathbf{m}_3, N_0\right)$ has a total of KM^3 stored values. Assume that each codeword for an uncoded SCMA system has an equal prior probability, i.e., $P\left(\mathbf{m}_1\right) = P\left(\mathbf{m}_2\right) = P\left(\mathbf{m}_3\right) = \frac{1}{M}$. Therefore, using the initial prior probability, equation (2.27) is the passed message from VN $\upsilon_1, \upsilon_2, \upsilon_3$ to FN l.

$$n^{\text{init}}_{\upsilon_1 \to l}\left(\mathbf{m}_1\right) = n^{\text{init}}_{\upsilon_2 \to l}\left(\mathbf{m}_2\right) = n^{\text{init}}_{\upsilon_3 \to l}\left(\mathbf{m}_3\right) = \frac{1}{M}. \tag{2.27}$$

Step 2: Message passing between FNs and VNs.

i. From FN to VN:

In this step, $\xi_l = \{\upsilon_1, \upsilon_2, \upsilon_3\}$ is RE l with the three connected users $\upsilon_1, \upsilon_2, \upsilon_3$. Equation (2.28) gives the message passed from the lth FN to VN υ_1

$$n_{l\to\upsilon_1}(\mathbf{m}_1)=\sum_{\mathbf{m}_2\in\mathbb{A}_2}\sum_{\mathbf{m}_2\in\mathbb{A}_3}\left(f\left(y_l\middle|\mathbf{m}_1,\mathbf{m}_2,\mathbf{m}_3,N_0\right)n_{\upsilon_2\to l}(\mathbf{m}_2)n_{\upsilon_3\to l}(\mathbf{m}_3)\right) \quad \textbf{(2.28)}$$
$$\text{for } \mathbf{m}_1\in\mathbb{A}_1$$

For the message passing from FN l to VN υ_1, the SPA multiplies $n_{\upsilon_2\to l}(\mathbf{m}_2)$ and $n_{\upsilon_3\to l}(\mathbf{m}_3)$ with FN l's likelihood function and then performs marginalization w.r.t υ_1. Equations (2.29) and (2.30) are the messages passed from FN l to VN υ_2 and FN l to VN υ_3, respectively.

$$n_{l\to\upsilon_2}(\mathbf{m}_2)=\sum_{\mathbf{m}_1\in\mathbb{A}_1}\sum_{\mathbf{m}_3\in\mathbb{A}_3}\left(f\left(y_l\middle|\mathbf{m}_1,\mathbf{m}_2,\mathbf{m}_3,N_0\right)n_{\upsilon_1\to l}(\mathbf{m}_1)n_{\upsilon_3\to l}(\mathbf{m}_3)\right), \quad \textbf{(2.29)}$$
$$\text{for } \mathbf{m}_2\in\mathbb{A}_2$$

$$n_{l\to\upsilon_3}(\mathbf{m}_3)=\sum_{\mathbf{m}_1\in\mathbb{A}_1}\sum_{\mathbf{m}_2\in\mathbb{A}_2}\left(f\left(y_l\middle|\mathbf{m}_1,\mathbf{m}_2,\mathbf{m}_3,N_0\right)n_{\upsilon_1\to l}(\mathbf{m}_1)n_{\upsilon_3\to l}(\mathbf{m}_3)\right) \quad \textbf{(2.30)}$$
$$\text{for } \mathbf{m}_3\in\mathbb{A}_3$$

Figure 2.8 shows the graphical representation of the message passing from FN l to VN υ_3. The received signal at FN l is a combination of all VN υ's possible values; thus, the received signal at VN υ is an assumption of the received message FN l.

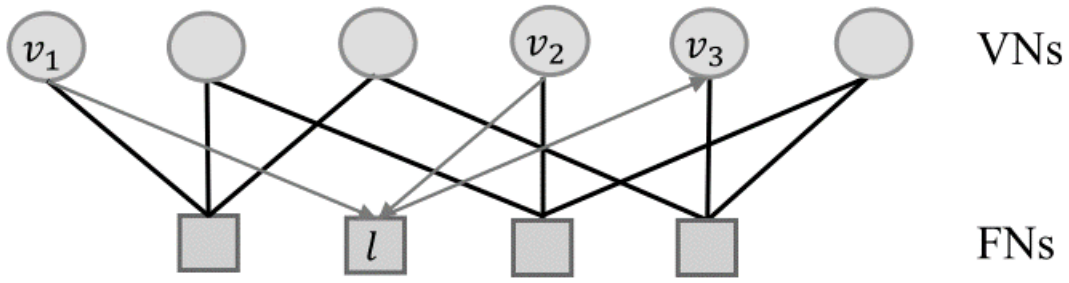

Figure 2.8: FN to VN Message Passing (Kschischang et al., 2001)

ii. From VN to FN

Assume $\zeta_\upsilon=\{l_1,l_2\}$, where VN υ's connected FNs are l_1 and l_2. Thus, equations (2.31) and (2.32) are the messages VN υ sent to FN l_1 and l_2, respectively.

$$n_{\upsilon\to l_1}(\mathbf{m}_\upsilon)=\text{normalize}\left(p_a(\mathbf{m}_\upsilon)n_{l_2\to\upsilon}(\mathbf{m}_\upsilon)\right), \quad \textbf{(2.31)}$$
$$\text{for } \mathbf{m}_\upsilon\in\mathbb{A}_\upsilon,$$

$$n_{\upsilon \to l_2}(\mathbf{m}_\upsilon) = \text{normalize}\left(p_a(\mathbf{m}_\upsilon) n_{l_1 \to \upsilon}(\mathbf{m}_\upsilon)\right), \quad \text{for } \mathbf{m}_\upsilon \in \mathbb{A}_\upsilon \tag{2.32}$$

where user υ's prior probability is p_a and $n_{\upsilon \to l_2}$ is VN υ's updates from the other connected FNs. The SPA normalizes equation (2.31) to ensure that the probability does not exceed 1, given by equation (2.33)

$$n_{\upsilon \to l_1}(\mathbf{m}_\upsilon) = \frac{p_a(\mathbf{m}_\upsilon) n_{l_2 \to \upsilon}(\mathbf{m}_\upsilon)}{\sum_{\mathbf{m}_\upsilon} n_{l_2 \to \upsilon}(\mathbf{m}_\upsilon)}, \quad \text{for } \mathbf{m}_\upsilon \in \mathbb{A}_\upsilon \tag{2.33}$$

The repetition of step 2 occurs until the number of iterations reaches N_{iter}, whereby the computed belief messages have no considerable change. Figure 2.9 shows the VN υ to FN l_2 message passing

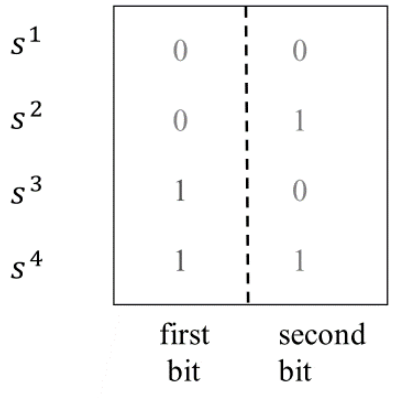

Figure 2.9: Bit-by-Bit Decoding

Step 3: Termination and codeword selection

On completion of step 2, the SPA computes each VN's final belief message, given by equation (2.34)

$$I_{\upsilon}\left(\mathbf{m}_{\upsilon}\right)=p_{a}\left(\mathbf{m}_{\upsilon}\right)n_{l_1\to\upsilon}\left(\mathbf{m}_{\upsilon}\right)n_{l_2\to\upsilon}\left(\mathbf{m}_{\upsilon}\right)\quad \text{for } \mathbf{m}_{\upsilon}\in\mathbb{A}_{\upsilon} \tag{2.34}$$

The SPA calculates the probability of all the codewords at each VN, where the chosen codeword for that user is the one with the most significant probability.

Alternatively, the estimated transmitted symbol can be obtained by calculating the bit LLR from $I_{v}\left(\mathbf{m}_{v}\right)$. Equation (2.35) gives the b_i^{th} bit LLR for VN υ, where the bits per symbol is b

$$\begin{aligned} LLR_{b_i}^{\upsilon} &= \log\frac{P\left(b_i=0\right)}{P\left(b_i=1\right)}, \\ &= \log\frac{\sum_{\mathbf{m}_{\upsilon}|b_i=0} I_{\upsilon}\left(\mathbf{m}_{\upsilon}\right)}{\sum_{\mathbf{m}_{\upsilon}|b_i=1} I_{\upsilon}\left(\mathbf{m}_{\upsilon}\right)} \end{aligned} \tag{2.35}$$

There are two bits per symbol when $M=4$; Therefore, the codewords and their corresponding symbols of user $\mathbf{m}_{\upsilon}$ are $\mathbb{A}_{\upsilon}=\left\{\mathbf{m}_{\upsilon}^{1},\mathbf{m}_{\upsilon}^{2},\mathbf{m}_{\upsilon}^{3},\mathbf{m}_{\upsilon}^{4}\right\}$ and $\left\{s^{1},s^{2},s^{3},s^{4}\right\}$, respectively. The SPA uses equation (2.34) and calculates each codeword's final belief messages, after which equation (2.36) gives the LLR's first bit

$$LLR_{b_1}^{\upsilon}=\log\frac{P\left(b_1=0\right)}{P\left(b_1=1\right)},=\log\frac{I_{\upsilon}\left(\mathbf{m}_{\upsilon}^{1}\right)+I_{\upsilon}\left(\mathbf{m}_{\upsilon}^{2}\right)}{I_{\upsilon}\left(\mathbf{m}_{\upsilon}^{3}\right)+I_{\upsilon}\left(\mathbf{m}_{\upsilon}^{4}\right)}. \tag{2.36}$$

Figure 2.9 shows the first bits of symbols s^1 and s^2 is 0, and s^3 and s^4 is 1, respectively. The computed belief message's ratio of the corresponding codeword $\mathbf{m}_{\upsilon}^{1},\mathbf{m}_{\upsilon}^{2}$ and $\mathbf{m}_{\upsilon}^{3},\mathbf{m}_{\upsilon}^{4}$ gives the first bit LLR. Therefore, if $P\left(b_1=1\right)>P\left(b_1=0\right)$ or if $LLR_{b_1}^{\upsilon}<0$, then the decoded value for the symbol's first bit is 1; otherwise, it is 0. Equation (2.37) gives the symbol's second bit

$$LLR_{b_2}^{\upsilon} = \log \frac{I_{\upsilon}\left(\mathbf{m}_{\upsilon}^{1}\right) + I_{\upsilon}\left(\mathbf{m}_{\upsilon}^{3}\right)}{I_{\upsilon}\left(\mathbf{m}_{\upsilon}^{2}\right) + I_{\upsilon}\left(\mathbf{m}_{\upsilon}^{4}\right)}. \quad \textbf{(2.37)}$$

2.2.7.1.2 Max-Log-SPA for SCMA Decoding:

The comparison between the MAP algorithm and SPA shows that the latter is less complex. However, there are other complexities with the message passing since the exponential and product operations become computationally demanding during the decoding process. Thus, employing the max-log-MPA algorithm from (Ameur et al., 2019) can simplify the MPA, like the max-log-MAP algorithm in (Robertson et al., 1995).

The use of the Jacobian logarithm in the max-log-SPA algorithm for SCMA decoding allows for further simplification of the sum-product algorithm. This is achieved by bypassing the need for exponential operations, which can be computationally complex and time-consuming. Instead, the logarithm is applied to the messages passed between the function nodes (FNs) and variable nodes (VNs) in the decoding system, allowing for more efficient calculation of the maximum likelihood function of the received signal.

This approach has been shown to improve the performance of the decoding process, particularly in cases where the received signal is degraded by noise or interference (Zhang et al., 2018; Chen et al., 2017). By simplifying the calculations required for the SPA using the Jacobian logarithm, the max-log-SPA algorithm is able to provide more accurate recovery of the transmitted data, with reduced calculation complexity and improved decoding performance.

$$\log\left(\exp\left(a_1\right) + \cdots + \exp\left(a_J\right)\right) \approx \max\left(a_1, \cdots, a_J\right). \quad \textbf{(2.38)}$$

The following steps show the max-log-SPA algorithm for the SCMA system:

Step 1: Initialisation

Equation (2.39) is the calculated LLR given **y** and **H**

$$\log\left(f\left(y_l\left|\mathbf{m}_1,\mathbf{m}_2,\mathbf{m}_3,N_0\right.\right)\right)=\frac{-1}{N_0}\left\|y_l-\begin{pmatrix}h_{l1}C_{l1}\left(\mathbf{m}_1\right)+\\ h_{l2}C_{l2}\left(\mathbf{m}_2\right)+\\ h_{l3}C_{l3}\left(\mathbf{m}_3\right)\end{pmatrix}\right\|^2. \quad \textbf{(2.39)}$$

$$\text{for } \mathbf{m}_1\in\mathbb{A}_1,\mathbf{m}_2\in\mathbb{A}_2,\mathbf{m}_3\in\mathbb{A}_3$$

VN υ to FN l's initial message given by equation (2.40)

$$n_{\upsilon\to l}^{\text{init}}=\log\left(n_{\upsilon\to l}^{\text{init}}\right)=\log\left(\frac{1}{M}\right). \quad \textbf{(2.40)}$$

Step 2: Message Passing between FNs and VNs

i. From FN to VN

The application of the logarithm to equation (2.28) in the message passing algorithm for SCMA decoding has been shown to improve the performance of the decoding process by reducing calculation complexity (Zhang et al., 2018; Chen et al., 2017). This equation represents the message passed from the lth function node to the variable node, and is given by:

$$\begin{aligned}a_i&=\log\left(f\left(y_l\left|\mathbf{m}_1,\mathbf{m}_2,\mathbf{m}_3,N_0\right.\right)n_{\upsilon_2\to l}\left(\mathbf{m}_2\right)n_{\upsilon_3\to l}\left(\mathbf{m}_3\right)\right)\\&=\log\left(f\left(y_l\left|\mathbf{m}_1,\mathbf{m}_2,\mathbf{m}_3,N_0\right.\right)\eta_{\upsilon_2\to l}\left(\mathbf{m}_2\right)\eta_{\upsilon_3\to l}\left(\mathbf{m}_3\right)\right),\end{aligned} \quad \textbf{(2.41)}$$

where $f\left(y_l\left|\mathbf{m}_1,\mathbf{m}_2,\mathbf{m}_3,N_0\right.\right)$ is the likelihood function of the received signal $y_l, n_{\upsilon_2\to l}\left(\mathbf{m}_2\right)$ and $n_{\upsilon_3\to l}\left(\mathbf{m}_3\right)$ are the incoming messages from the neighbouring function nodes υ_2 and υ_3, respectively, and $\mathbf{m}_1$, $\mathbf{m}_2$, and $\mathbf{m}_3$ are the messages from the neighbouring variable nodes.

The implementation of this equation in the message passing algorithm is shown in equation (2.38), where equation (2.42) represents the passed message from the l^{th} FN to VN υ:

$$\eta_{l\to\upsilon_1}^{\text{init}}(\mathbf{m}_1)=\max_{\mathbf{m}_2,\mathbf{m}_3}\begin{pmatrix}\log\left(f\left(y_l|\mathbf{m}_1,\mathbf{m}_2,\mathbf{m}_3,N_0\right)\right)\\+\eta_{\upsilon_2\to l}(\mathbf{m}_2)+\eta_{\upsilon_3\to l}(\mathbf{m}_3)\end{pmatrix}. \quad \textbf{(2.42)}$$

for $\mathbf{m}_1\in\mathbb{A}_1$

Equation (2.43) gives the message passed from FN l to VN υ_2

$$\eta_{l\to\upsilon_2}^{\text{init}}(\mathbf{m}_2)=\max_{\mathbf{m}_1,\mathbf{m}_3}\begin{pmatrix}\log\left(f\left(y_l|\mathbf{m}_1,\mathbf{m}_2,\mathbf{m}_3,N_0\right)\right)\\+\eta_{\upsilon_1\to l}(\mathbf{m}_1)+\eta_{\upsilon_3\to l}(\mathbf{m}_3)\end{pmatrix}. \quad \textbf{(2.43)}$$

for $\mathbf{m}_2\in\mathbb{A}_2$

Equation (2.44) gives the message passed from FN l to VN υ_3

$$\eta_{l\to\upsilon_3}^{\text{init}}(\mathbf{m}_3)=\max_{\mathbf{m}_1,\mathbf{m}_3}\begin{pmatrix}\log\left(f\left(y_l|\mathbf{m}_1,\mathbf{m}_2,\mathbf{m}_3,N_0\right)\right)\\+\eta_{\upsilon_1\to l}(\mathbf{m}_1)+\eta_{\upsilon_2\to l}(\mathbf{m}_2)\end{pmatrix}. \quad \textbf{(2.44)}$$

for $\mathbf{m}_3\in\mathbb{A}_3$

ii. From VN to FN

Each user utilizes more than one REs to send data; thus, the log of the passed messages (by applying the logarithm to equations (2.31) and (2.32)) from the (2.31) and (2.32))) from the υ th VN to FN l_1 is given by equation (2.45), and the υ th VN to FN l_2 is given by equation (2.46).

$$\eta_{\upsilon\to l_1}(\mathbf{m}_\upsilon)=\log\left(\frac{1}{M}\right)+\eta_{l_2\to\upsilon}(\mathbf{m}_\upsilon), \quad \textbf{(2.45)}$$

for $\mathbf{m}_\upsilon\in\mathbb{A}_\upsilon$

$$\eta_{\upsilon\to l_2}(\mathbf{m}_\upsilon)=\log\left(\frac{1}{M}\right)+\eta_{l_1\to\upsilon}(\mathbf{m}_\upsilon). \quad \textbf{(2.46)}$$

for $\mathbf{m}_\upsilon\in\mathbb{A}_\upsilon$

Step 3: Termination and selection of codewords

Step 2 iterates for N times before calculating the log APP for each user's codeword as,

$$\log\left(I_\upsilon\left(\mathbf{m}_\upsilon\right)\right)=\log\left(\frac{1}{M}\right)+\eta_{l_1\to\upsilon}\left(\mathbf{m}_\upsilon\right)+\eta_{l_2\to\upsilon}\left(\mathbf{m}_\upsilon\right) \quad \text{for } \mathbf{m}_\upsilon\in\mathbb{A}_\upsilon \tag{2.47}$$

From equation (2.35) and (2.38), the bit LLR of the b^{th} bit is given by equation (2.48)

$$LLR_{b_i}^{\upsilon}=\max_{\mathbf{m}_\upsilon|b_i=0}\left(\log\left(I_\upsilon\left(\mathbf{m}_\upsilon\right)\right)\right)-\max_{\mathbf{m}_\upsilon|b_i=1}\left(\log\left(I_\upsilon\left(\mathbf{m}_\upsilon\right)\right)\right). \tag{2.48}$$

The LLR of the symbol's first bit is given by equation (2.49)

$$LLR_{b_1}^{\upsilon}=\max_{\mathbf{m}_\upsilon^1,\mathbf{m}_\upsilon^2}\left(\log\left(I_\upsilon\left(\mathbf{m}_\upsilon^1\right)+I_\upsilon\left(\mathbf{m}_\upsilon^1\right)\right)\right)-\max_{\mathbf{m}_\upsilon^3,\mathbf{m}_\upsilon^4}\left(\log\left(I_\upsilon\left(\mathbf{m}_\upsilon^3\right)+I_\upsilon\left(\mathbf{m}_\upsilon^4\right)\right)\right). \tag{2.49}$$

If the $LLR_{b_1}^{\upsilon}<0$, the decoded value of the symbol's first bit is 1; otherwise, it is 0. Similarly, equation (2.50) gives the second bit LLR

$$LLR_{b_2}^{\upsilon}=\max_{\mathbf{m}_\upsilon^1,\mathbf{m}_\upsilon^3}\left(\log\left(I_\upsilon\left(\mathbf{m}_\upsilon^1\right)+I_\upsilon\left(\mathbf{m}_\upsilon^3\right)\right)\right)-\max_{\mathbf{m}_\upsilon^2,\mathbf{m}_\upsilon^4}\left(\log\left(I_\upsilon\left(\mathbf{m}_\upsilon^2\right)+I_\upsilon\left(\mathbf{m}_\upsilon^4\right)\right)\right). \tag{2.50}$$

If the $LLR_{b_2}^{\upsilon}<0$, the decoded value of the symbol's second bit is 1; otherwise, it is 0.

The max-log-SPA algorithm for SCMA decoding simplifies the sum-product algorithm by applying the Jacobian logarithm to the messages passed between the FNs and VNs in the decoding system. This allows for more efficient calculation of the maximum likelihood function of the received signal, improving the performance of the decoding process. The use of the logarithm has been shown to be particularly effective in cases where the received signal is degraded by noise or interference (Zhang et al., 2018; Chen et al., 2017). By simplifying the calculations required for the SPA using the Jacobian logarithm, the max-log-SPA algorithm is able to provide more accurate recovery of the transmitted data with reduced calculation complexity.

2.3 Summary

The fundamental principles of the SCMA communication are presented in the chapter. First an overview of the SCMA uplink system model is discussed and then the decoders used to identify superimposed user information.

3.1 Introduction

In this chapter, we present an optimization method for the constellation design of a mother constellation. The focus of this thesis is to optimize this critical parameter in order to minimize the probability of error in communication over an additive white Gaussian noise (AWGN) channel.

3.2 Constellation model over AWGN channel

As shown in Figure 4.1, a user sends a symbol $\bar{x} = [x_1, x_2, x_3, ..., x_n]$ that is negatively affected by the AWGN channel. The receiver attempts to recover the received symbol $\bar{r}$ optimally. It is assumed that bit 0 is assigned to $\hat{x}_1$ and bit 1 to $\hat{x}_2$. The k[th] symbol transmitted on resource n is given by $s_n^{(k)} \in \left\{\tilde{x}_1, \tilde{x}_2\right\}$, where $(1 \le i \le 2)$. The received symbol is given by:

$$\bar{r}_n = s_n^{(k)} + \bar{\omega}_n. \tag{3.1}$$

To minimize the probability of error, it is critical to optimize the minimum distance between neighbouring constellation points. We will discuss this relationship in more detail in the following sections.

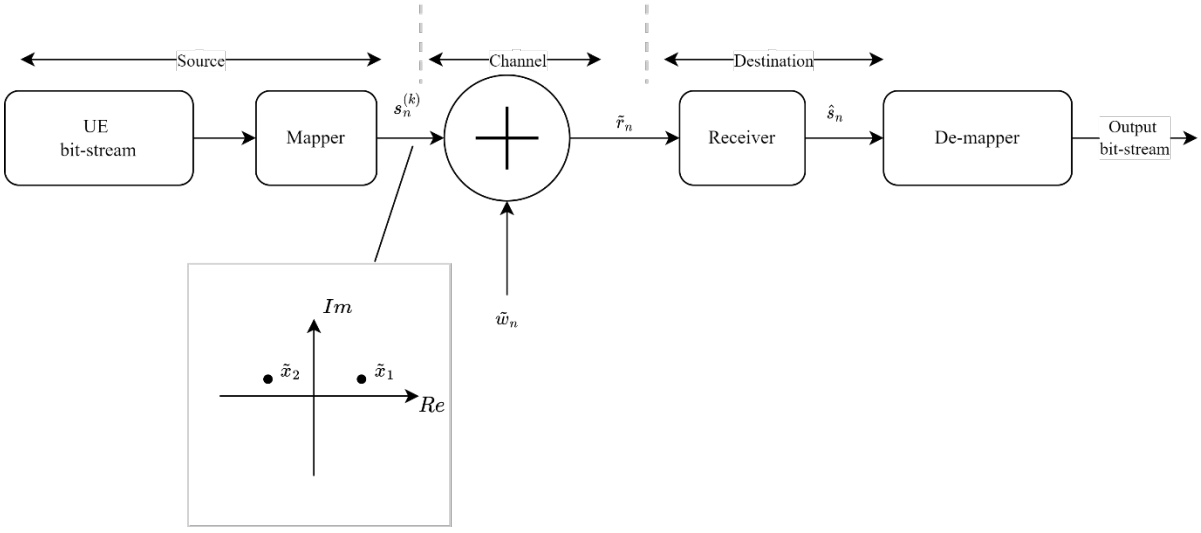

Figure 3.1: Simple digital communication system with the transmitted constellation

Here $\tilde{\omega}_n$ denote samples of a complex-wide sense stationary (WSS), additive white Gaussian noise (AWGN) with zero mean and variance

$$\sigma_{\omega}^{2} = \frac{1}{2} E\left[\left| \tilde{\omega}_{n} \right|^{2} \right]. \tag{3.2}$$

The assumed statistical independence of the real and imaginary leads to the following:

$$E\left[\omega_{n,\mathrm{Re}} \omega_{n,\mathrm{Im}} \right] = E\left[\omega_{n,\mathrm{Re}} \right] E\left[\omega_{n,\mathrm{Im}} \right] = 0. \tag{3.3}$$

Thus, with zero-mean, the complex Gaussian random variable is expressed by the circular normal distribution $\mathcal{CN}\left(0, 2\sigma_{\omega}^{2}\right)$. The normal distribution arguments are the mean and variance over two dimensions. Furthermore, the complex random variable consists of two dimensions. Therefore, it is assumed that:

$$E\left[\omega_{n,\mathrm{Re}}^{2} \right] = E\left[\omega_{n,\mathrm{Im}}^{2} \right] = \sigma_{\omega}^{2}. \tag{3.4}$$

Autocorrelation of $\tilde{\omega}_{n}$ is expressed as:

$$\begin{aligned} \tilde{R}_{\tilde{\omega}\tilde{\omega}}\left(m\right) &\triangleq \frac{1}{2} E\left[\tilde{\omega}_{n} \tilde{\omega}_{n-m}^{*} \right], \\ &= \sigma_{\omega}^{2} \delta_{K}\left(m\right) \end{aligned} \tag{3.5}$$

where the Kronecker delta function is given by:

$$\delta_{K}\left(m\right) \triangleq \begin{cases} 1, & \text{if } m = 0 \\ 0, & \text{otherwise.} \end{cases} \tag{3.6}$$

At the receiver, a decision is made between the two constellation points in Figure 3.1. The average probability of error can be presented as follows:

$$\begin{aligned} P_{e}\left(\tilde{x}_{k}, \tilde{r}_{n}\right) &= P\left(\tilde{x}_{k} \text{ not sent} \middle| \tilde{r}_{n}\right) \\ &= 1 - P\left(\tilde{x}_{k} \text{ sent} \middle| \tilde{r}_{n}\right) \\ &\text{ or concilely} \\ &= 1 - P\left(\tilde{x}_{k} \middle| \tilde{r}_{n}\right). \end{aligned} \tag{3.7}$$

From equation (3.7), to minimize the probability of error (P_e), intuitively, $\tilde{x}_k$ needs to be maximized. Thus, the receiver computes the probabilities of $P(\tilde{x}_1|\tilde{r}_n)$ and $P(\tilde{x}_2|\tilde{r}_n)$ to decide the largest outcome. The estimated signal can be written as:

$$\hat{s}_n = \tilde{x}_k, P(\tilde{x}_k|\tilde{r}_n).$$

The above estimate is well known as the *maximum a-posteriori* (MAP) estimate or a MAP receiver. By applying Bayes' rule to the MAP detector receiver equation above:

$$\max_k \frac{p(\tilde{r}_n|\tilde{x}_k)P(\tilde{x}_k)}{P(\tilde{r}_n)} = \max_k \frac{p(\tilde{r}_n|\tilde{x}_k)P(\tilde{x}_k)}{\sum_k p(\tilde{r}_n|\tilde{x}_k)P(\tilde{x}_k)}. \quad \textbf{(3.8)}$$

$P(.)$ and $p(.)$ denotes probability and the probability density function (PDF), respectively. Independence is achieved by constellation points being equally likely, resulting in $P(\tilde{x}_k)$ being constant and independent of *k.* Also, $\sum_k p(\tilde{r}_n|\tilde{x}_k)P(\tilde{x}_k)$ is independent of *k.* Under these conditions, the MAP receiver detector is viewed as a maximum likelihood (ML) receiver detector.

$$\max_k p(\tilde{r}_n|\tilde{x}_k). \quad \textbf{(3.9)}$$

Equation (3.9) finds the maximum conditional pdf of $\tilde{r}_n$ given $\tilde{a}_i$, and is Gaussian. Thus, it can be represented as:

$$\max_k \frac{1}{2\pi\sigma_\omega^2} \exp\left(-\frac{|\tilde{r}_n - \tilde{x}_k|^2}{2\sigma_\omega^2}\right). \quad \textbf{(3.10)}$$

Applying the natural logarithm to equation (3.10) and omitting the constants which are negligible. The following is found:

$$\min_k |\tilde{r}_n - \tilde{x}_k|^2. \quad \textbf{(3.11)}$$

The above equation (3.11) denotes the ML receiver detector method of inference. The constellation points closest to the received point $\tilde{r}_n$ will be chosen as the sent information.

3.2.1 Analysis of detector performance

The correlation between the receiver detector and the constellation is analysed by computing the ML detector probability of error, given that $\tilde{x}_1$ was transmitted. The following equation describes the circumstances under which this would occur:

$$\left|\tilde{r}_n - \tilde{x}_1\right|^2 < \left|\tilde{r}_n - \tilde{x}_2\right|^2. \tag{3.12}$$

Equation (3.12) can be simplified to the following form:

$$\left|\tilde{d} + \tilde{\omega}_n\right|^2 < \left|\tilde{\omega}_n\right|^2. \tag{3.13}$$

Equation (3.13) implies:

$$\left|\tilde{d}\right|^2 + 2\,\mathrm{Re}\left\{\tilde{d}^*\tilde{\omega}_n\right\} < 0, \tag{3.14}$$

where '*' indicates the complex conjugate and $\tilde{d} = \tilde{x}_1 - \tilde{x}_2$.

Let

$$\begin{aligned} Z &= 2\,\mathrm{Re}\left\{\tilde{d}^*\tilde{\omega}_n\right\} \\ &= 2\left(d_{\mathrm{Re}}\tilde{\omega}_{n,\mathrm{Re}} + d_{\mathrm{Im}}\tilde{\omega}_{n,\mathrm{Im}}\right) \end{aligned}, \tag{3.15}$$

Im and *Re* denote the imaginary and real elements. The linear combination of two real Gaussian random variables indicates that *Z* is also a real Gaussian random variable. The mean of *Z* is,

$$E[Z] = 0, \tag{3.16}$$

and the variance:

$$\begin{aligned} E\left[Z^2\right] &= 4\delta_\omega^2\left|\tilde{d}\right|^2 \\ &= \delta_Z^2 \end{aligned}. \tag{3.17}$$

Thus, the probability of error is expressed as:

$$\begin{aligned} P\left(Z < \left|\tilde{d}\right|^2\right) &= \int_{Z=-\infty}^{-\left|\tilde{d}\right|^2} \frac{1}{\delta_Z \sqrt{2\pi}} \exp\left(-\frac{Z^2}{2\delta_Z^2}\right) \mathrm{d}Z \\ &= \frac{1}{2}\operatorname{erfc}\left(\sqrt{\frac{\left|\tilde{d}\right|^2}{8\delta_\omega^2}}\right) \\ &= P\left(\tilde{x}_2 \left| \tilde{x}_1\right.\right) \end{aligned} \quad . \tag{3.18}$$

Note that:

$$\operatorname{erfc}(x) = \frac{2}{\sqrt{\pi}} \int_{y=x}^{\infty} \exp\left(-y^2\right) dy \, . \tag{3.19}$$

The above equation is the complementary error function which takes values:

$$\begin{aligned} &\operatorname{erfc}(-\infty) = 2 \\ &\operatorname{erfc}(0) = 1 \\ &\operatorname{erfc}(\infty) = 0 \\ &\operatorname{erfc}(-x) = 2 - \operatorname{erfc}(x) \end{aligned} \quad . \tag{3.20}$$

From the above equations, it is evident that the minimum distance contributes to the critical performance of the probability of error. Furthermore, P_e is independent of the rotation and translation of the constellation. It is this feature that will be implemented in the optimization of the chosen mother constellations in the upcoming chapters.

3.3 Design of a 16-Point Signal Constellation

The authors (Sklar Bernard, 2016; Tranter et al., 2003; David Falconer, 2011; Rice, 2009) discussed the design and optimization of 16-point constellation used in QAM and APSK systems. These constellation points are an essential component of modern communication systems, and there exists a plethora of possibilities when designing them.

3.3.1 Optimum Ring Ratio

The 16-point constellation has many possibilities for choosing a ring ratio (*RR*). In (Binh, 2017), the authors showed a relationship between using the theoretical best *RR* to minimize P_e and maximizing the MED between neighbouring constellation points in an AWGN channel. Furthermore, the MED is maximized when

$$d_1 = d_2 = R_2 - R_1 = \text{MED}. \tag{3.21}$$

Implementing geometrical manipulation yields the following:

$$\text{MED} = 2R_1 \cdot \sin\left(\frac{\pi}{4}\right). \tag{3.22}$$

Thus, the optimum *RR* is given by:

$$RR_{opt} = \frac{R_2}{R_1} = \frac{\left(\text{MED} + R_1\right)}{R_1} = \frac{\left(2 \cdot R_1 \cdot \sin\left(\frac{\pi}{4}\right) + R_1\right)}{R_1} \approx 1.77. \tag{3.23}$$

The optimum ring ratio is independent of the average power, as shown in the equation below:

$$P_0 = \frac{\left(8R_1^{\,2} + 8R_2^{\,2}\right)}{16} = \frac{\left(R_1^{\,2} + R_2^{\,2}\right)}{2}. \tag{3.24}$$

Therefore, the approximate relationship between MED and P_0 is given by:

$$\text{MED} \approx 0.53 \cdot \sqrt{P_0}. \tag{3.25}$$

The above theory is implemented when optimizing the ring ratio of the mother constellation for the design of SCMA codebooks.

3.4 Summary

The implication of choosing optimal constellations for transmission over an AWGN channel is discussed. By maximizing the minimum Euclidean distance between neighbouring points, the receiver can reduce the probability of making an error. Thus (3.21) and (3.23) are the fundamental technique used to optimize the mother constellation. This theory is implemented as a design optimization technique.

4.1 Introduction

This chapter considers the research question on how SCMA codebooks can be optimally constructed using APSK and 16-QAM constellations to enhance the spectral efficiency and bit error rate performance of uplink transmission from multiple users while achieving a reduced complexity.

4.2 Mother Constellation Selection

The low-density structure and multi-dimensional constellations of SCMA codebooks have contributed to exceptional SCMA system performance and high spectral efficiency. The fundamental component of a good codebook design is the selected mother constellation with a large MED. Thus, sub-constellations derived from partitioning the mother constellation into four sub-constellations to increase the MED are proposed. The increased MED improves decoding complexity at the receiver and reduces inter-user interference on the subcarriers.

4.2.1 Codebook Design Optimization Modelling

The MED is a critical parameter of the mother constellation that impacts the performance of an SCMA system. Maximizing the MED translates to reducing the inter-user interference on subcarriers and consequently improving decoding reliability. Thus, a large MED establishes the need to select an efficient mother constellation when designing an SCMA codebook. The optimization objectives are selecting an efficient mother constellation and then partitioning the mother constellation into sub-constellations.

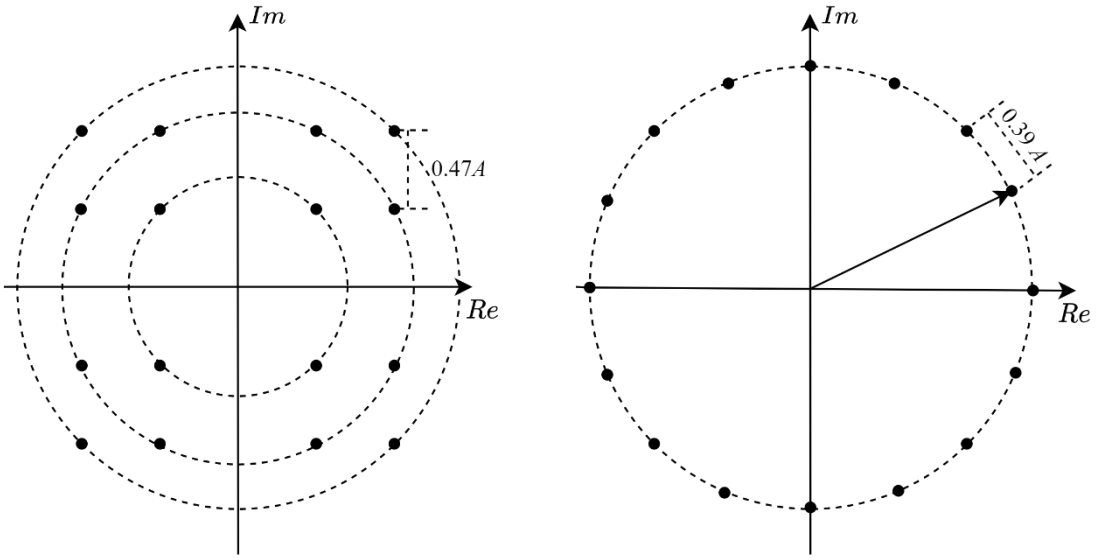

(a) 16-QAM (b) 16-PSK

Figure 4.1: Comparing High Order Modulation Schemes

Figure 4.1 shows the high-order constellation of the traditional 16-QAM and 16-PSK. The focus here is to examine the MEDs of each constellation. The minimum Euclidean distance is defined as:

$$\text{MED} = \min\left\{\sqrt{\left|x_i - x_j\right|^2 + \left|y_i - y_j\right|^2}\right\}, i \neq j\,. \tag{4.1}$$

The calculated MEDs of constellations in Figure 4.1 are determined using, (4.1) as

$$\text{MED} = 0.47A,\ \text{16-QAM},$$

$$\text{MED} = 0.39A,\ \text{16-PSK},$$

where A represents the constellations' maximum amplitude. The QAM modulation has a larger MED of $0.47A$ compared to $0.39A$ and therefore, is chosen over the 16-PSK modulation. The QAM modulation has several forms, namely square, round, and uneven round. These different forms are due to the selected amplitudes and phases, yielding different MEDs.

The constellation partitioning based SCMA codebook design steps are as follows:

i. Optimize the minimum Euclidean distance (MED) of the chosen constellation by implementing equation (3.22).
ii. Perform constellation partitioning to increase the MED of the constellations.
iii. Use the signature matrix to allocate resource elements to users.
iv. Assign sub-constellations from partitioning to users using a permutation matrix to avoid repetition over the same resource element.
v. The resultant user codebooks are then used to encode user data.
vi. Send the user-encoded information to the base station over different channels and perform superposition at the base station.
vii. Use ideal channel information to equalize the received signal and pass it to the multi-user detector (MUD).
viii. Implement max-log-MAP decoding on the received data.

Development of sub-constellations by partitioning

The advantage of SCMA systems is the ability to support multiple users on a single resource element using sparse coding schemes (Sklar Bernard, 2016; Rappaport, 2002; Rice, 2009; David Falconer, 2011). This allows for the overloading of resources, which can improve system efficiency. The diverse sub-constellation points also enhance the reliable decoding of user codewords that are superimposed on a single resource element at the receiver (Sklar Bernard, 2016; Rappaport, 2002; Rice, 2009; David Falconer, 2011).

To generate the sub-constellations, we must first consider the bit sequence length, b, of a single user for transmission at a given time interval. The number of required constellation points can then be determined using the following equation:

$$M = 2^b, \tag{4.2}$$

where M denotes the number of constellation points. This equation allows for the calculation of the number of constellation points needed for a given bit sequence length, which is an important in the design of the SCMA codebook.

The condition for reliable decoding of information at the receiver is given by equation (4.3) (Sklar Bernard, 2016; Rappaport, 2002; Rice, 2009; David Falconer, 2011):

$$d_f \leq J_k, \tag{4.3}$$

where d_f is the number of sub-constellations and J_k s the total number of users sharing a resource element. Based on the number of user collisions in the signature matrix **F** and conditions set by equation (4.3) the required number of sub-constellations can be computed. Furthermore, the number of constellation points on each resource is given by MJ_k (Sklar Bernard, 2016; Rappaport, 2002; Rice, 2009; David Falconer, 2011).

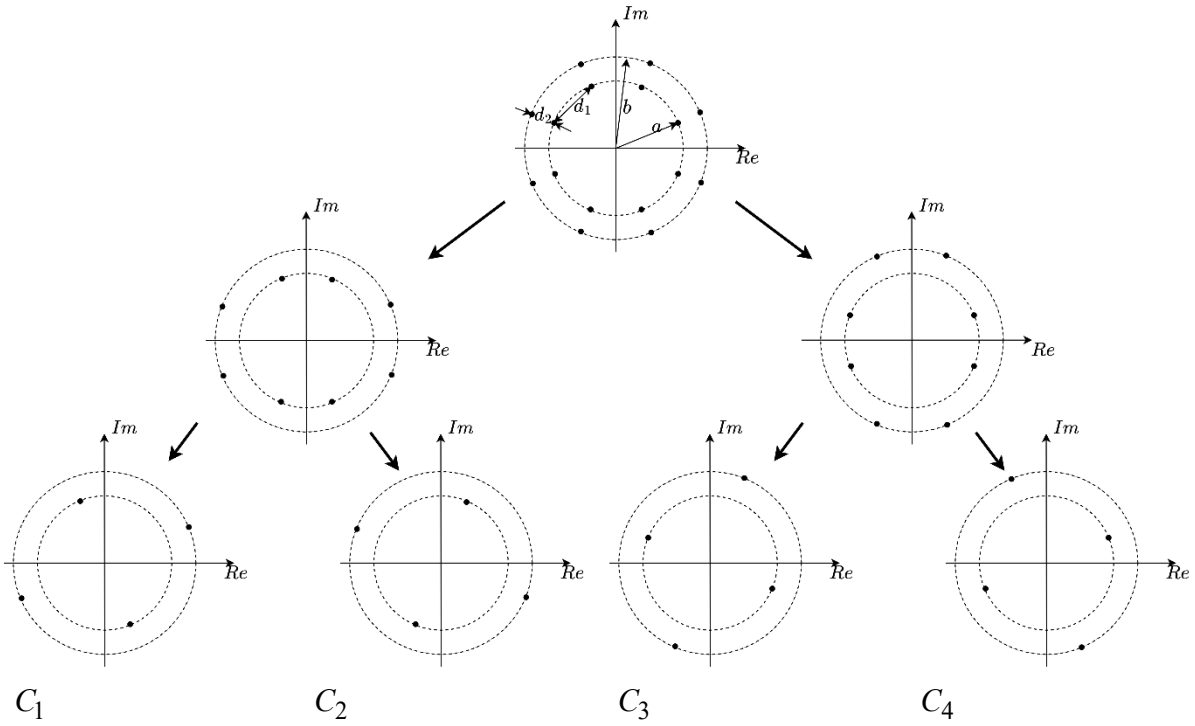

Figure 4.2: Sub-constellation by Mother Constellation PartitioningFigure 4.2 shows an example of partitioning the mother constellation. The first-order partitioning of the mother constellation generates two sub-constellations. Partitioning is subsequently performed on the two generated sub-constellation to produce a total of four sub-constellations, which satisfies the condition set by (4.3) for reliable decoding at the receiver.

SCMA Codebook Generation by Mapping Sub-Constellation

The sub-constellations generated by partitioning the mother constellation can be represented by the set (Liu et al., 2018):

$$C_{sub,i} = \left\{ S_{1,i}, S_{2,i}, ..., S_{d_f,i} \right\}, \tag{4.4}$$

where $i = 1, 2, ..., N/d_f$ and N is the total number of constellation points of the mother constellation. The mother constellation ($\mathbf{A}'_{MC}$) is represented by the sub-matrix $C_{i,j}^{sub}$, where i and j denotes the resource elements and user respectively. Thus, with the aid of the signature matrix, the sub-constellation, allocated to user j and resource i is defined as (Liu et al., 2018):

$$C_{i,j}^{sub} = \begin{cases} S_i^p, & F_{i,j} = 1 \\ 0, & F_{i,j=0} \end{cases}, \tag{4.5}$$

where S_i^p is the p^{th} value after permutation of random ordering of the set $\left\{ S_{1,i}, S_{2,i}, ..., S_{d_f,i} \right\}$. The non-zero elements in the factor graph **F** are replaced with S_i^p. Combining the permuted sets with the message bits m_j of order $\log_2(M)$ over a specified resource element i and user j. The final codebook defined as (Liu et al., 2018):

$$C_{i,j}(m_j) = \begin{cases} S_i^p(m_j), & F_{i,j} = 1 \\ 0, & F_{i,j=0} \end{cases}, j \in [1, J]. \tag{4.6}$$

Equation (4.5) and (2.3) are used to allocate the sub-constellations to resource elements. Table 4-1 shows one of many possible results due to random permutation of the sub-constellations.

Table 4-1: Permutation of Sub-Constellations

	UE1	**UE2**	**UE3**	**UE4**	**UE5**	**UE6**
RE1	C_2	C_3	C_1	0	0	0
RE2	C_4	0	0	C_2	C_1	0
RE3	0	C_1	0	C_4	0	C_3
RE4	0	0	C_2	0	C_4	C_1

Each sub-constellation $\{C_1, C_2, C_3, C_4\}$ consist of codewords $\{00, 01, 10, 11\}$ presented by complex constellation points. Table 4-1 shows a combination of sub-constellations that have been uniquely allocated to users and resource elements. This emphasizes the importance of

using permutation sub-constellations across REs to ensure uniqueness and enable accurate decoding. By assigning unique permutations of sub-constellations to each user and RE, the receiver can accurately decode the codewords transmitted by each user, even if they are superimposed on the same RE. This is essential for reliable communication in SCMA systems. By using permutation sub-constellations, we can ensure that each user's codewords are uniquely encoded and can be accurately decoded at the receiver.

Equation (4.6) describes the allocation of codewords to users and resource elements in an SCMA system. For example, the term $C_{i,3}(4)$ denotes the fourth codeword of user 3's sub-constellations on the REs. Figure 4.2 shows that the fourth codeword exists in quadrant four for all sub-constellations. This means that the fourth codeword of each user's sub-constellation is in the same quadrant on the constellation diagram. This is an important property of the SCMA system, as it allows the receiver to accurately decode the transmitted codewords. By assigning codewords to the same quadrant for each user, we can ensure that the codewords are uniquely encoded and can be accurately decoded at the receiver.

Table 4-2: Demonstrates the information (4.6) denotes across the REs

	UE_3
	11
RE_1	$C_1(4)$
RE_2	0
RE_3	0
RE_4	$C_2(4)$

Also, $C_{1,3}(m_3)$ denotes the sub-constellation points that exist on RE_1 of UE_3 and describes the sub-constellation points of the allocated to codewords $\{00,01,10,11\}$.

Table 4-3: Demonstrates the information (4.6) denotes across a RE_1.

	UE_3			
	00	01	10	11
RE_1	$C_1(1)$	$C_1(2)$	$C_1(3)$	$C_1(4)$

4.3 Summary

The chapter discusses the technique used to design SCMA codebooks by partitioning the mother constellation into sub-constellations. The sub-constellations are allocated to UEs and permutations are utilized to assign unique combinations of sub-constellations across REs. The

unique distribution of sub-constellations facilitates decoding accuracy of the received information on a RE.

Chapter 5 SCMA CODEBOOK DESIGN BASED ON STAR 16-QAM CONSTELLATION PARTITIONING

5.1 Introduction

The previous chapter discusses the optimization used on the mother constellation to design SCMA codebooks for uplink transmission. This chapter implements the theory discussed in Chapters 3 to Chapter 5. The star 16-QAM is a commonly used signal constellation in communication systems. This chapter implements the star 16-QAM constellation as the chosen mother constellation. More specifically, the conventional 2A-8P Star 16-QAM consists of two-amplitude-level and eight-phase states. The system model consists of six users allocated resource elements for uplink transmission to a receiver.

5.2 System Model

Evaluation and implementation of the uplink SCMA codebook design by authors (Liu et al., 2018) has led to the chosen design and scheme implementation.

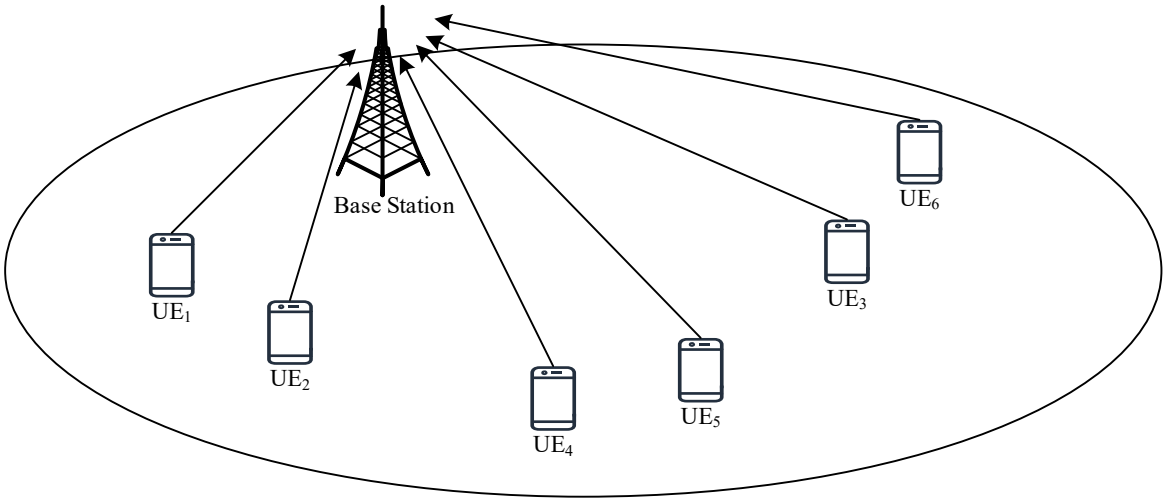

Figure 5.1: Uplink SCMA Communication System Model

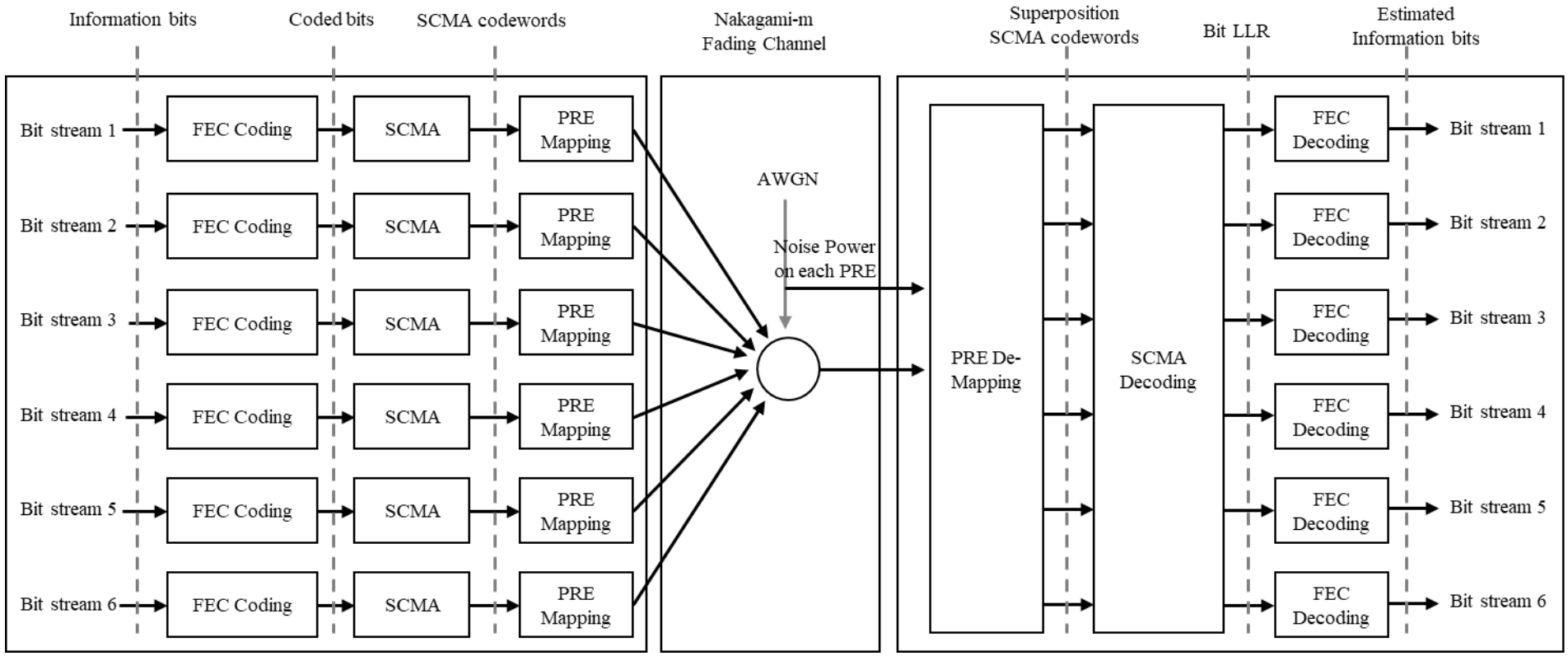

Figure 5.2 System Block Diagram of SCMA Uplink Model

5.2.1 Channel Model

The Rayleigh, Rician and Nakagami fading models are widely used in the analysis of wireless communication systems to describe the fading of signals that propagate through a multipath environment. The fading of signals can be modelled as a random process and the severity of fading can be described by the distribution of the amplitude of the signal.

The Rayleigh fading model is a statistical representation of signal fading that occurs due to random phase changes between different paths. The amplitude of the signal in the Rayleigh model is modelled as a Rayleigh random variable with probability density function (pdf) given by:

$$f_R(x) = \frac{x}{\sigma^2} e^{-\frac{x^2}{2\sigma^2}} \tag{5.1}$$

where x is the amplitude of the signal and σ^2 is the variance of the fading.

The Rician fading model is used to describe fading in a scenario where there is a strong direct path and weaker reflected paths. The amplitude of the signal in the Rician model is modelled as a non-central chi-square random variable with two degrees of freedom and pdf given by:

$$f_{Ri}(x) = \frac{x}{\sigma^2} e^{-\frac{(x+K^2)}{2\sigma^2}} I_0(\frac{xK}{\sigma^2}) \tag{5.2}$$

where K is the Rician K-factor, which represents the ratio of the power of the direct path to the power of the scattered paths.

The Nakagami fading model is a generalization of the Rayleigh and Rician models and represents fading in an environment with a mixture of strong and weak paths. The amplitude of the signal in the Nakagami model is modelled as a Nakagami random variable with pdf given by:

$$f_N(x) = \frac{2x^{2m-1}}{\Gamma(m)\Omega^{2m}} e^{-\frac{x^2}{\Omega^2}} \tag{5.3}$$

where m is the shape parameter and Ω^2 is the scale parameter. These models provide a mathematical framework for describing the behaviour of wireless communication signals in different multipath environments. The parameters of these models determine the fading severity and distribution, which are important for characterizing the wireless communication channel and optimizing system performance.

5.2.2 Proposed SCMA Codebook Design based on Star 16-QAM

To detect the different users, the phase and amplitude need to be determined. Many combinations exist with the possibility of using two amplitudes and eight phases. However, in this analysis, the star 16-QAM is made of sixteen symbols equally distributed between two amplitudes. The phase difference between each point on the same ring is $\pi/4$.

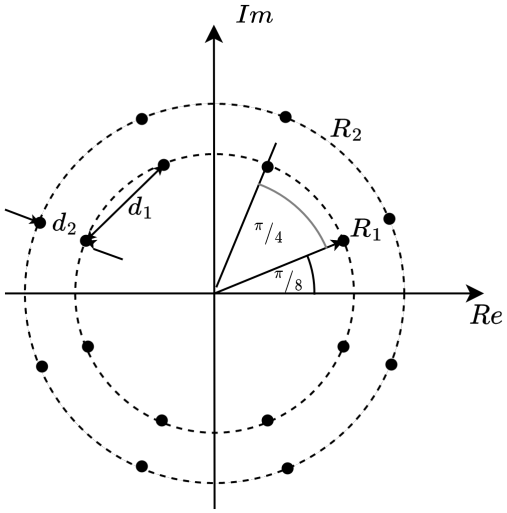

Figure 5.3: Conventional Star 16-QAM Mother Constellation

The mother constellation $\left(\mathbf{A}_{MC}^{'}\right)$ is chosen to be the conventional star 16-QAM and defined as:

$$\mathbf{A}_{MC}^{'}=\begin{cases}\left[R_1\cos\left(\dfrac{(2k-1)\pi}{8}\right),R_1\sin\left(\dfrac{(2k-1)\pi}{8}\right)\right],1\le k\le 8,\\ \left[R_2\cos\left(\dfrac{(2k-1)\pi}{8}\right),R_2\sin\left(\dfrac{(2k-1)\pi}{8}\right)\right],1\le k\le 8.\end{cases} \quad \textbf{(5.4)}$$

Optimization of the constellation in Figure 5.3 is implemented by optimizing the ring ratio (*RR*) defined as:

$$RR=\frac{R_2}{R_1}, \quad \textbf{(5.5)}$$

where R_1 and R_2 are the inner and outer radii, respectively. Optimization of the *RR* is implemented to maximize the minimum Euclidean distance (MED) or between the neighbouring constellations points.

The author in (Binh, 2017) defines the optimization problem as:

$$d_1 = d_2 = R_2 - R_1 = \text{MED}. \tag{5.6}$$

Implementing some geometric manipulation $d_{\min}$:

$$\text{MED} = 2R_1 \sin(\pi/8). \tag{5.7}$$

Furthermore, the optimal *RR* is found to be:

$$RR_{opt} = \frac{R_2}{R_1} = \frac{(\text{MED} + R_1)}{R_1} = \frac{(2R_1 \sin(\pi/8) + R_1)}{R_1} \approx 1.77. \tag{5.8}$$

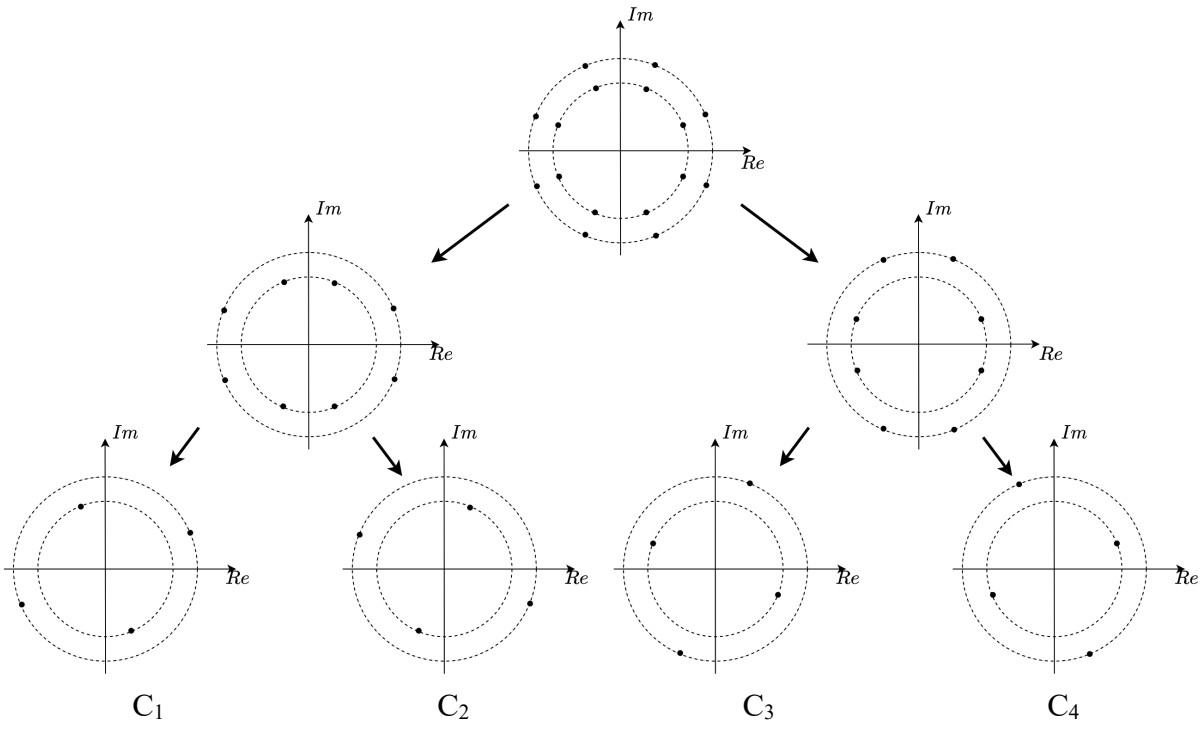

Figure 5.4: Conventional Star 16-QAM Mother Constellation Partitioning

Figure 5.4 shows that the mother constellation ($\mathbf{A}'_{MC}$) is partitioned into four sub-constellations. By applying random permutation to the sub-constellations from (4.5) and (2.3) the sub-constellations are randomly allocated to resource elements. Shown in Table 5-1 is one of many possible results due to random permutation of the sub-constellations.

Table 5-1 Permutation and Signature Matrix Output

	UE1	**UE2**	**UE3**	**UE4**	**UE5**	**UE6**
RE1	C1	C2	C4	0	0	0
RE2	C3	0	0	C1	C4	0
RE3	0	C4	0	C2	0	C3
RE4	0	0	C2	0	C3	C1

5.2.3 Analysis of the proposed partitioned 16-QAM SCMA Constellation

The average signal energy (E) for the system model is fixed at 8.8 and used in conjunction with the RR_{opt} to find the amplitude of R_1 and R_2. The average signal energy is usually defined as:

$$E = \frac{1}{M}\sum_{i=1}^{M}\|x_i\|^2 . \tag{5.9}$$

Thus, the average signal energy is given by:

$$\begin{aligned} E &= \frac{1}{16}\left(8R_1^2 + 8R_2^2\right) \\ &= \frac{1}{16}\left(8R_1^2 + 8R_1^2 RR_{\text{opt}}\right) \end{aligned} . \tag{5.10}$$

Making R_1 the subject of (5.10):

$$\begin{aligned} R_1 &= \sqrt{\frac{16E}{8+8RR_{\text{opt}}}} \\ &= \sqrt{\frac{16\cdot 8.8}{8+8\cdot 1.7654}} \\ &= 2.0677 \end{aligned} .$$

R_2 is found by the product of R_1 and RR_{opt} and found to be 3.6503. The larger *MED* of the conventional 16-QAM constellation, made it an ideal mother constellation candidate. Figure 5.4 shows the resultant sub-constellations after partitioning the star 16-QAM. The optimal ring

ratio was found to be 1.77, which resulted in the larger minimum Euclidean distance between neighbouring constellation points of sub-constellations in Table 5-2:

Table 5-2: Partitioning Increases MED of sub-constellations

$\mathbf{A}'_{MC}$	C_1	C_2	C_3	C_4
2.54	4	4	4	4

Table 5-3 shows the resultant SCMA codebook for the chosen mother constellation with average signal energy fixed at 8.8.

Table 5-3: Partitioned Star 16-QAM SCMA Codebook

USER	USER CODEBOOKS
1	$\begin{bmatrix} 1.9103 + 0.7913i & -1.3969 + 3.3724i & -1.9103 - 0.7913i & 1.3969 - 3.3724i \\ 3.3724 + 1.3969i & -0.7913 + 1.9103i & -3.3724 - 1.3969i & 0.7913 - 1.9103i \\ 0.0000 + 0.0000i & 0.0000 + 0.0000i & 0.0000 + 0.0000i & 0.0000 + 0.0000i \\ 0.0000 + 0.0000i & 0.0000 + 0.0000i & 0.0000 + 0.0000i & 0.0000 + 0.0000i \end{bmatrix}$
2	$\begin{bmatrix} 0.7913 + 1.9103i & -3.3724 + 1.3969i & 0.7913 - 1.9103i & 3.3724 - 1.3969i \\ 0.0000 + 0.0000i & 0.0000 + 0.0000i & 0.0000 + 0.0000i & 0.0000 + 0.0000i \\ 1.3969 + 3.3724i & -1.9103 + 0.7913i & -1.3969 - 3.3724i & 1.9103 - 0.7913i \\ 0.0000 + 0.0000i & 0.0000 + 0.0000i & 0.0000 + 0.0000i & 0.0000 + 0.0000i \end{bmatrix}$.
3	$\begin{bmatrix} -1.9103 + 0.7913i & 1.3969 + 3.3724i & 1.9103 - 0.7913i & -1.3969 - 3.3724i \\ 0.0000 + 0.0000i & 0.0000 + 0.0000i & 0.0000 + 0.0000i & 0.0000 + 0.0000i \\ 0.0000 + 0.0000i & 0.0000 + 0.0000i & 0.0000 + 0.0000i & 0.0000 + 0.0000i \\ -3.3724 + 1.3969i & 0.7913 + 1.9103i & 3.3724 - 1.3969i & -0.7913 - 1.9103i \end{bmatrix}$
4	$\begin{bmatrix} 0.0000 + 0.0000i & 0.0000 + 0.0000i & 0.0000 + 0.0000i & 0.0000 + 0.0000i \\ 1.9103 + 0.7913i & -1.3969 + 3.3724i & -1.9103 - 0.7913i & 1.3969 - 3.3724i \\ 0.7913 + 1.9103i & -3.3724 + 1.3969i & -0.7913 - 1.9103i & 3.3724 - 1.3969i \\ 0.0000 + 0.0000i & 0.0000 + 0.0000i & 0.0000 + 0.0000i & 0.0000 + 0.0000i \end{bmatrix}$
5	$\begin{bmatrix} 0.0000 + 0.0000i & 0.0000 + 0.0000i & 0.0000 + 0.0000i & 0.0000 + 0.0000i \\ -1.9103 + 0.7913i & 1.3969 + 3.3724i & 1.9103 - 0.7913i & -1.3969 - 3.3724i \\ 0.0000 + 0.0000i & 0.0000 + 0.0000i & 0.0000 + 0.0000i & 0.0000 + 0.0000i \\ -0.7913 + 1.9103i & 3.3724 + 1.3969i & 0.7913 - 1.9103i & -3.3724 - 1.3969i \end{bmatrix}$
6	$\begin{bmatrix} 0.0000 + 0.0000i & 0.0000 + 0.0000i & 0.0000 + 0.0000i & 0.0000 + 0.0000i \\ 0.0000 + 0.0000i & 0.0000 + 0.0000i & 0.0000 + 0.0000i & 0.0000 + 0.0000i \\ -0.7913 + 1.9103i & 3.3724 + 1.3969i & 0.7913 - 1.9103i & -3.3724 - 1.3969i \\ -1.3969 + 3.3724i & 1.9103 + 0.7913i & 1.3969 - 3.3724i & -1.9103 - 0.7913i \end{bmatrix}$

5.3 Numerical Simulations and Results Analyses of the proposed SCMA Codebook and Max-Log-MPA decoder

In this section the SCMA codebook performance is compared with existing codebook designs in (Liu et al., 2018), and (Nikopour & Baligh, 2013), the undivided 16-QAM SCMA codebook in (Yu et al., 2016) and the trellis coded modulation SCMA subset division based on 16-QAM in (Nikopour & Baligh, 2013). The parameters in Table 5-4 are based on the system model parameters in (Liu et al., 2018).

Table 5-4: System Model Parameters

Parameters	Values
Channel type	Nakagami-*m* with m=2 Rayleigh m=1
Number of symbols/frames	4096
Number of cycles	1000
Number of users	6
Number of REs	4
Number of iterations	15
Overload factor	1.5
Average Energy	8.8

With the above parameters Figure 5.5 shows the experimental outcome of BER of different proposed SCMA codebooks in a Nakagami fading channel.

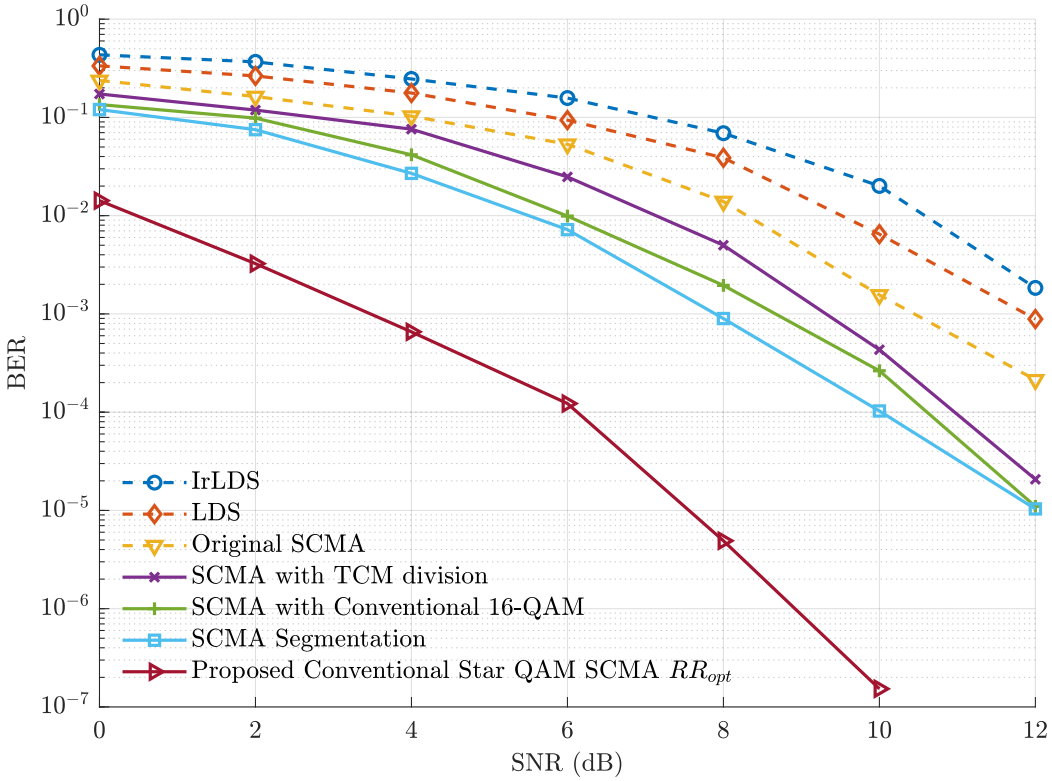

Figure 5.5: BER Comparison Among Existing Codebook Designs

Results in Figure 5.5 show that the proposed design outperforms the existing codebook designs at low SNR. At BER=10^{-4} dB , the proposed SCMA codebook design outperforms the existing designs. Specifically, the proposed codebook design yields a 3.9 dB performance gain as compared to the SCMA segmented codebook in (Liu et al., 2018). More so, the proposed SCMA codebook design shows considerable performance gain of 4.9 dB, 5.3 dB, 6.4 dB, 7.4 dB, and 7.9 dB as compared to (Yu et al., 2015), (Liang et al., 2017), and the LDS and IrLDS schemes in (Cheng et al., 2015) respectively.

The performance increase in BER can be explained by the larger MED of 4, which is achieved by choosing an optimal mother constellation and performing constellation partitioning on the mother constellation. Applying (4.1) the MED in (Liu et al., 2018), (Yu et al., 2015), and (Liang et al., 2017) are revealed to have the values of 2.11, 1.7654, 1.414 respectively.

The values of authors (Cheng et al., 2015) are difficult to calculate and are marked as not applicable. Table 5-5 puts the MED into perspective and compares the SNR at a given BER of 10^{-4}.

Table 5-5: BER Comparison of MED among different SCMA Codebooks

Codebooks	MED	SNR at BER of 10^{-4} (dB)	BER Gain (dB)
Proposed SCMA Codebook	4	6.1	
Segmented SCMA Codebook	2.11	10	3.9
SCMA with 16-QAM	1.765	11	4.9
SCMA with TCM division	1.414	11.4	5.3
Original SCMA	1	12.5	6.4
LDS	N/A	13.5	7.4
IrLDS	N/A	14	7.9

Furthermore, the increased MED of sub-constellations are larger than the mother constellation. Thus, reducing collisions among user information bits when mapped to a sparse codewords transmitted over a RE. The diversity by allocating users different codebooks across the same RE contributes to the BER performance as it guarantees decoding accuracy.

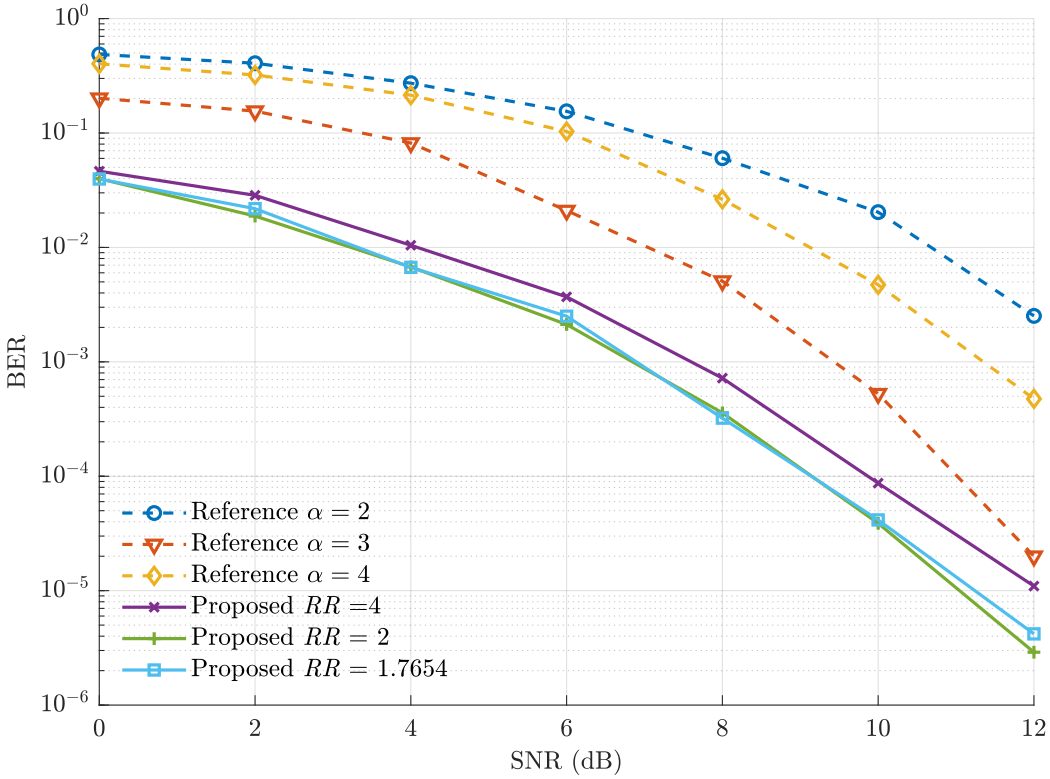

Figure 5.6: Rayleigh Fading Channel SCMA Codebook Performance

Figure 5.6 compares the effect of changing the *RR* of the SCMA codebooks over a Rayleigh fading channel. As expected, the low fading coefficient of m=1 has degraded the performance of the designed SCMA codebooks. The proposed Conventional Star 16-QAM with $RR_{\text{opt}} = 1.7654$ displays a BER performance of more than 3 dB at BER = 10^{-4} over the SCMA codebook in (Liu et al., 2018). Figure 5.6 also shows the BER performance between the

designed scheme with different RR over the Rayleigh channel. The result shows that $RR_{\text{opt}} = 1.7654$ has a better BER performance compared to $RR = 4$ at high and low SNR. The 1 dB improvement at BER = 10^{-4} shows the importance of designing codebooks with neighbouring constellation points equidistant as defined by (3.21).

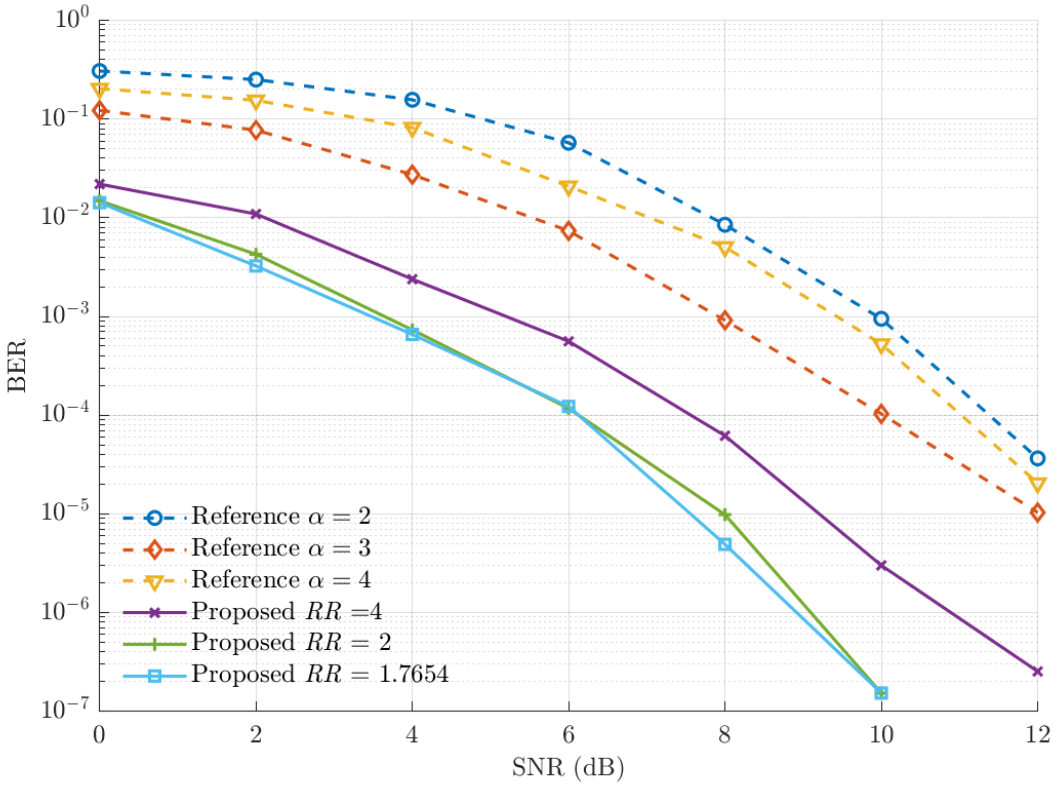

Figure 5.7: Nakagami Fading Channel Performance of SCMA Codebooks

Figure 5.7 presents the BER performance of the proposed SCMA codebook design over a Nakagami-m fading channel, with m=2. A further BER improvement of 3.9 dB at 10^{-4} over the proposed design in (Liu et al., 2018) is achieved. The proposed RR_{opt} is shown to surpass $RR = 4$ by nearly 2 dB at BER=10^{-4}.

5.4 Summary

This chapter executes all theory learnt from earlier chapters, by implementing ring ratio optimization of the mother constellation. Also, implementation of partitioning the mother constellations into sub-constellations result in an increased MED. The SCMA codebooks for uplink transmission and numerical simulation results are discussed.

Chapter 6 DUAL RING STAR 16-QAM CONSTELLATION PARTITIONING BASED SCMA CODEBOOK

6.1 Introduction

The following chapter presents a dual ring star 16-QAM modulation scheme. The principles of previous chapters are applied for this SCMA codebook design. Furthermore, SCMA codebook is designed using the Dual Ring Star 16-QAM constellation. Optimisation of the *RR* is executed by calculating the *RR* that ensures equidistance between neighbouring constellation points.

When compared with the amplitude shift keying (ASK) modulation, 16-QAM is able to reduce the symbols rate by four times that required by ASK modulation (Binh, 2008). The author reports the importance of ring ratios as the transition of amplitude levels of Star QAM constellation patterns critically affects the error detection. Authors (Yang et al., 2014) shares the same opinion on ring ratios, where they proposed a scheme to make sure all neighbouring constellation points are equidistant from each other.

6.2 Dual Ring Star 16-QAM SCMA Codebook Design

Figure 6.1 shows the construction of the Dual Ring Star 16 QAM constellation which consists of two amplitudes and 16 phases. The constellation is defined by:

$$\mathbf{A}_{MC}^{'}=\begin{cases}\left[R_1\cos\left(\frac{(2k-1)\pi}{8}\right),R_1\sin\left(\frac{(2k-1)\pi}{8}\right)\right],1\le k\le 8,\\ \left[R_2\cos\left(\frac{(k-1)\pi}{4}\right),R_2\sin\left(\frac{(k-1)\pi}{4}\right)\right],1\le k\le 8,\end{cases}.$$

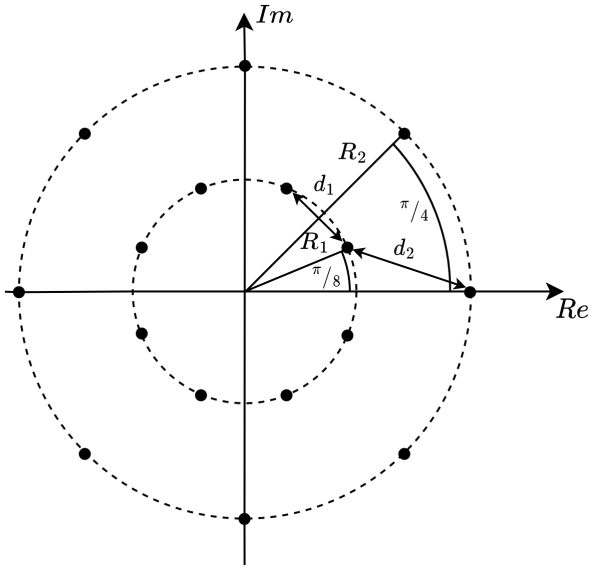

Figure 6.1: Dual Star 16-QAM Mother Constellation

Optimization of the constellation in Figure 6.1 is implemented by optimizing the ring ratio (*RR*) defined as:

$$RR = \frac{d_2}{d_1}, \tag{6.1}$$

where R_1 and R_2 are the inner and outer radii, respectively. Optimization of the *RR* is implemented to maximize the minimum Euclidean distance (MED) between the neighbouring constellations points.

The author (Binh, 2017) defines the optimization problem as:

$$d_1 = d_2 = R_2 - R_1 = \text{MED}. \tag{6.2}$$

Implementing some trigonometric manipulation to find RR_{opt} using (6.2):

$$\begin{aligned} d_1 = d_2 &= \sqrt{\left|R_1\cos(\pi/8) - R_1\cos(3\pi/8)\right|^2 + \left|R_1\sin(\pi/8) - R_1\sin(3\pi/8)\right|^2} \\ &= \sqrt{\left|R_1\cos(\pi/8) - R_2\cos(0)\right|^2 + \left|R_1\sin(\pi/8) - R_2\sin(0)\right|^2} \end{aligned}. \tag{6.3}$$

Also, solving for RR_{opt} using (6.1) which satisfies (6.3):

$$RR_{\text{opt}} \approx 1.5867 .$$

The partitioning of the mother constellations is presented in Figure 6.2. Two steps are followed as in Chapter 6, where partitioning is employed and meets the conditions set by (4.3).

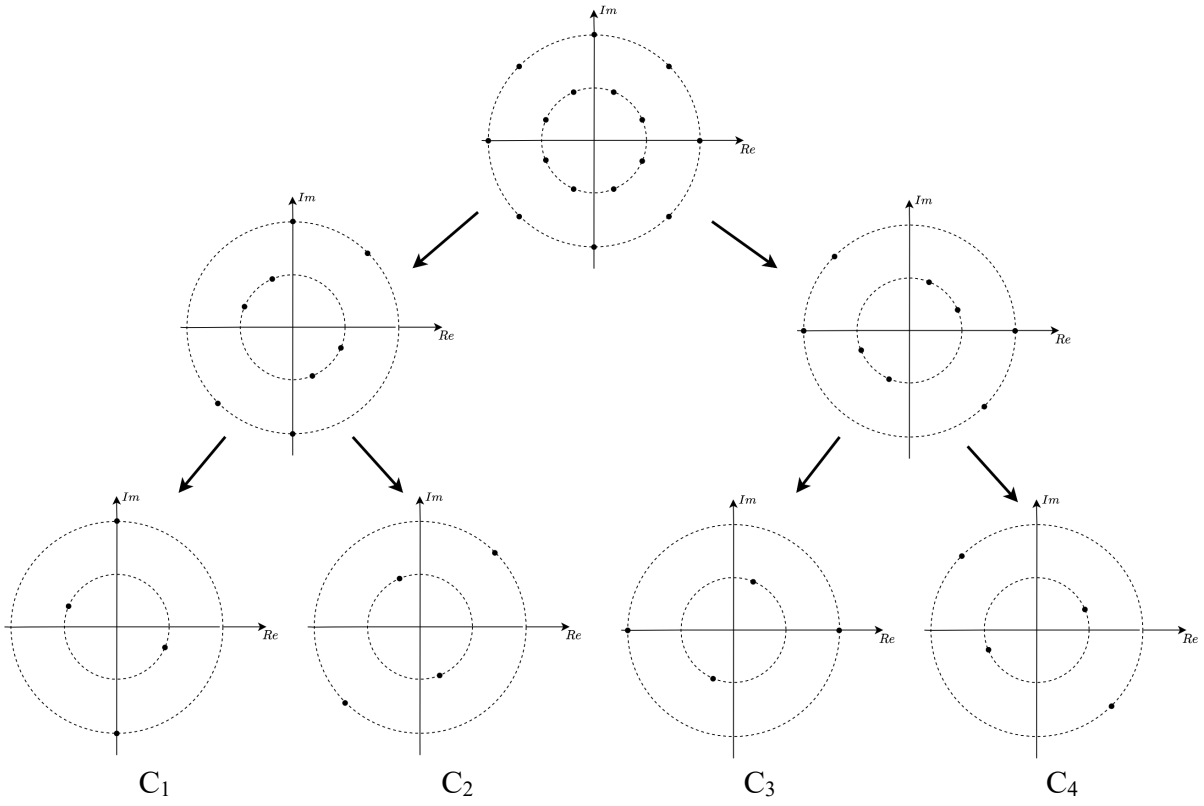

Figure 6.2: Dual Star 16-QAM Mother Constellation Partitioning

By applying random permutation to the sub-constellations from (4.5) and (2.3) the sub-constellations are randomly allocated to resource elements. Table 6-3 shows one of several possible results due to random permutation of the sub-constellations.

Table 6-1 Permutation and Signature Matrix Output

	UE1	**UE2**	**UE3**	**UE4**	**UE5**	**UE6**
RE1	C2	C3	C1	0	0	0
RE2	C4	0	0	C1	C2	0
RE3	0	C4	0	C3	0	C1
RE4	0	0	C2	0	C1	C4

6.2.1 Analysis of the proposed partitioned Dual Star 16-QAM SCMA Constellation

The average signal energy (E) for the system model is fixed at 8.8 and used to in conjunction with the RR_{opt} to find the amplitude of R_1 and R_2. The average signal energy is usually defined as: R_1

$$E = \frac{1}{M}\sum_{i=1}^{M}\|x_i\|^2 . \tag{6.4}$$

Thus, the average signal energy is given by:

$$\begin{aligned} E &= \frac{1}{16}\left(8R_1^2 + 8R_2^2\right) \\ &= \frac{1}{16}\left(8R_1^2 + 8R_1^2 RR_{\text{opt}}\right) \end{aligned} . \tag{6.5}$$

Making R_1 the subject of (5.10) :

$$\begin{aligned} R_1 &= \sqrt{\frac{16E}{8+8RR_{\text{opt}}}} \\ &= \sqrt{\frac{16\cdot 8.8}{8+8\cdot 1.5867}} \\ &= 2.2368 \end{aligned} .$$

R_2 is found by the product of R_1 and RR_{opt} and found to be 3.5492. The larger MED of the conventional 16-QAM constellation, made it an ideal mother constellation candidate. The optimal ring ratio was found to be 1.5867, which resulted in the larger minimum Euclidean distance between neighbouring constellation points of sub-constellations in Table 5-2:

Table 6-2: Partitioning Increases MED of sub-constellations

$\mathbf{A}'_{MC}$	C_1	C_2	C_3	C_4
1.7120	3.3947	4.4736	4.4736	3.3947

Table 6-3 shows the resultant SCMA codebook for the chosen mother constellation with average signal energy fixed at 8.8.

Table 6-3: Proposed Dual Ring SCMA Codebook

USER	USER CODEBOOKS
1	$\begin{bmatrix} 0.0000 + 3.5492i & -2.0666 + 0.8560i & 0.0000 - 3.5492i & 2.0666 - 0.8560i \\ 2.0666 + 0.8560i & -2.5096 + 2.5096i & -2.0666 - 0.8560i & 2.5096 - 2.5096i \\ 0.0000 + 0.0000i & 0.0000 + 0.0000i & 0.0000 + 0.0000i & 0.0000 + 0.0000i \\ 0.0000 + 0.0000i & 0.0000 + 0.0000i & 0.0000 + 0.0000i & 0.0000 + 0.0000i \end{bmatrix}$
2	$\begin{bmatrix} 2.5096 + 2.5096i & -0.8560 + 2.0666i & -2.5096 - 2.5096i & 0.8560 - 2.0666i \\ 0.0000 + 0.0000i & 0.0000 + 0.0000i & 0.0000 + 0.0000i & 0.0000 + 0.0000i \\ 2.0666 + 0.8560i & -2.5096 + 2.5096i & -2.0666 - 0.8560i & 2.5096 - 2.5096i \\ 0.0000 + 0.0000i & 0.0000 + 0.0000i & 0.0000 + 0.0000i & 0.0000 + 0.0000i \end{bmatrix}$
3	$\begin{bmatrix} 0.8560 + 2.0666i & 3.5492 + 0.0000i & -0.8560 - 2.0666i & -3.5492 + 0.0000i \\ 0.0000 + 0.0000i & 0.0000 + 0.0000i & 0.0000 + 0.0000i & 0.0000 + 0.0000i \\ 0.0000 + 0.0000i & 0.0000 + 0.0000i & 0.0000 + 0.0000i & 0.0000 + 0.0000i \\ 0.0000 + 3.5492i & -2.0666 + 0.8560i & 0.0000 - 3.5492i & 2.0666 - 0.8560i \end{bmatrix}$
4	$\begin{bmatrix} 0.0000 + 0.0000i & 0.0000 + 0.0000i & 0.0000 + 0.0000i & 0.0000 + 0.0000i \\ 0.8560 + 2.0666i & 3.5492 + 0.0000i & -0.8560 - 2.0666i & -3.5492 + 0.0000i \\ 2.5096 + 2.5096i & -0.8560 + 2.0666i & -2.5096 - 2.5096i & 0.8560 - 2.0666i \\ 0.0000 + 0.0000i & 0.0000 + 0.0000i & 0.0000 + 0.0000i & 0.0000 + 0.0000i \end{bmatrix}$
5	$\begin{bmatrix} 0.0000 + 0.0000i & 0.0000 + 0.0000i & 0.0000 + 0.0000i & 0.0000 + 0.0000i \\ 0.0000 + 3.5492i & -2.0666 + 0.8560i & 0.0000 - 3.5492i & 2.0666 - 0.8560i \\ 0.0000 + 0.0000i & 0.0000 + 0.0000i & 0.0000 + 0.0000i & 0.0000 + 0.0000i \\ 0.8560 + 2.0666i & 3.5492 + 0.0000i & -0.8560 - 2.0666i & -3.5492 + 0.0000i \end{bmatrix}$
6	$\begin{bmatrix} 0.0000 + 0.0000i & 0.0000 + 0.0000i & 0.0000 + 0.0000i & 0.0000 + 0.0000i \\ 0.0000 + 0.0000i & 0.0000 + 0.0000i & 0.0000 + 0.0000i & 0.0000 + 0.0000i \\ 3.5492 + 0.0000i & 0.8560 + 2.0666i & -3.5492 + 0.0000i & -0.8560 - 2.0666i \\ 2.0666 + 0.8560i & -2.5096 + 2.5096i & -2.0666 - 0.8560i & 2.5096 - 2.5096i \end{bmatrix}$

6.3 Numerical Simulations and Results Analyses of the proposed Dual Ring Star 16-QAM SCMA Codebook.

As in Chapter 6 the SCMA codebook performance is compared with existing codebook designs in (Liu et al., 2018), and (Nikopour & Baligh, 2013), the undivided 16-QAM SCMA codebook in (Yu et al., 2016) and the trellis coded modulation SCMA subset division based on 16-QAM in (Nikopour & Baligh, 2013). The parameters in Table 6-4 is based on the system model in (Liu et al., 2018), which are used for simulations and results.

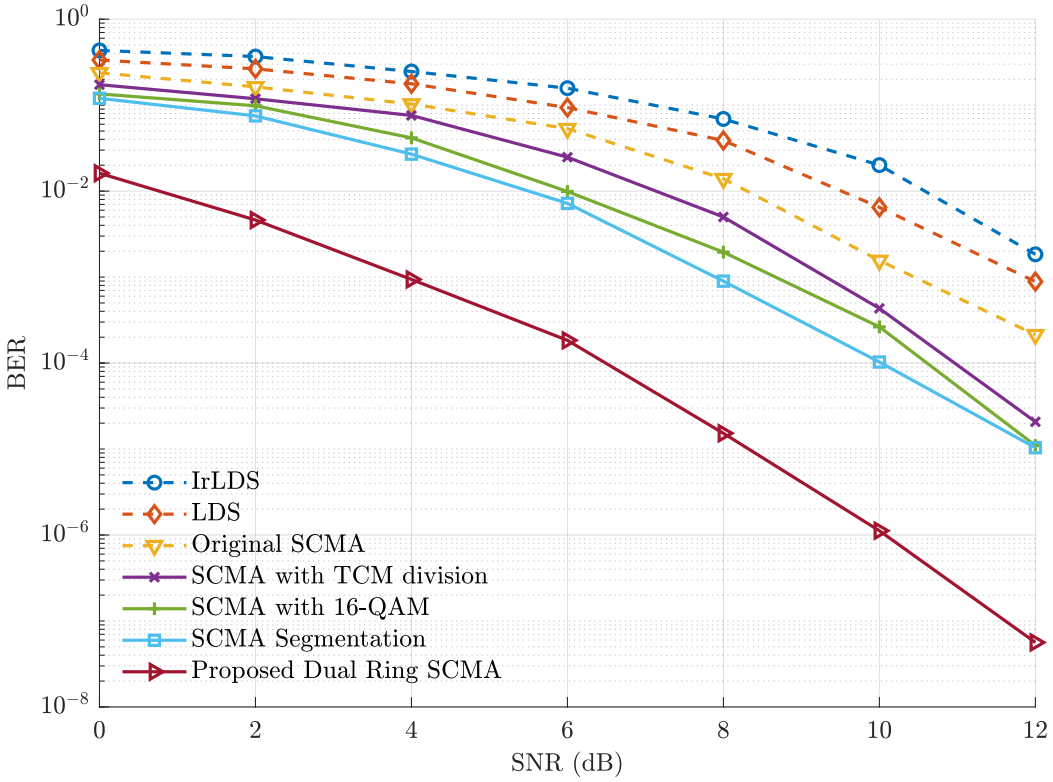

Figure 6.3: BER Comparison Among Existing Codebook Designs vs Proposed Dual Ring Mother Constellation

Results in Figure 6.3 show the proposed Dual Ring Star 16-QAM surpasses the existing SCMA codebook designs at low and high SNR. At SNR = 6.48 dB and BER=10^{-4} dB, the proposed SCMA codebook design outperforms all the existing designs. Specifically, the proposed codebook design yields a 3.52 dB BER performance gain as compared to the SCMA segmented codebook in (Liu et al., 2018). More so, the proposed Dual Ring Star 16-QAM SCMA codebook design shows considerable performance gain of 4.52 dB, 4.92 dB, 6.02 dB, 7.02 dB and 7.52 dB as compared to (Yu et al., 2015), (Liang et al., 2017), and the LDS and IrLDS schemes in (Cheng et al., 2015) respectively.

The performance increase in BER can be explained by the larger MED of 3.3947, which is achieved by choosing an optimal mother constellation and performing constellation partitioning on the mother constellation. Applying (4.1) the MEDS of authors (Liu et al., 2018), (Yu et al., 2015) and (Liang et al., 2017) are revealed to have the values of 2.11, 1.7654, 1.414 respectively.3..3947

Table 6-4 Comparison of MED among different SCMA Codebooks

Codebooks	MED	SNR at BER of 10^{-4} (dB)	BER Gain (dB)
Proposed SCMA Codebook	4	6.48	
Segmented SCMA Codebook	2.11	10	3.52
SCMA with 16-QAM	1.765	11	4.52
SCMA with TCM division	1.414	11.4	4.92
Original SCMA	1	12.5	6.02
LDS	N/A	13.5	7.02
IrLDS	N/A	14	7.52

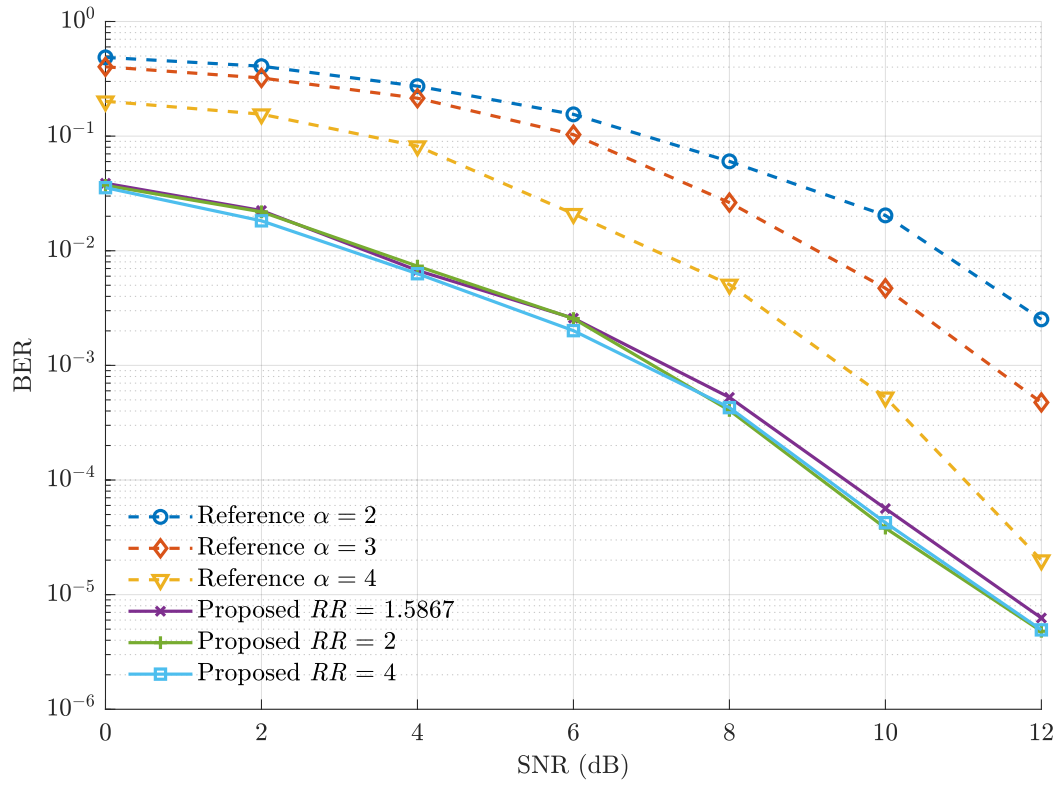

Figure 6.4: Rayleigh BER Comparison at different *RR*

Figure 6.4 compares the effect of changing the *RR* of the proposed SCMA codebook design over a Rayleigh fading channel. The proposed Dual Star 16-QAM with $RR_{\text{opt}} = 1.5867$ shows an improvement of approximately 2 dB at BER 10^{-4} over the SCMA codebook of (Liu et al., 2018). The BER performance between the designed scheme with different *RR* over the Rayleigh channel is also compared. The finding is $RR_{\text{opt}} = 1.5867$ shows a negligible BER improvement over *RR*=2 and *RR*=4.

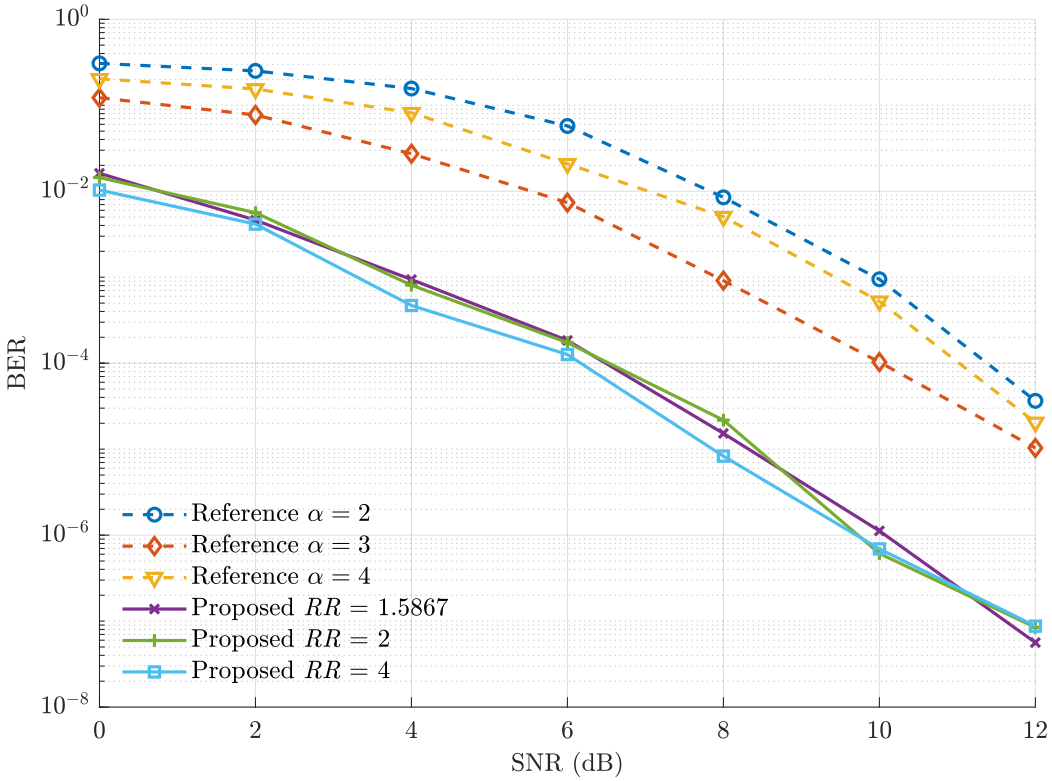

Figure 6.5: Nakagami Comparison BER performance with Different RR

Figure 6.5 illustrates the BER performance of the proposed SCMA codebook design over a Nakagami-m fading channel, with m=2. A further BER improvement of 3.52 dB at 10^{-4} over the proposed design in (Liu et al., 2018) is achieved. The proposed RR_{opt} and $RR = 4$ display nearly equivalent BER performances. Though at high SNR the optimal ring ratio does begin to display marginal BER performance gain over $RR = 4$. The proposed design illustrates the importance of having a large MED as this does correlate to the BER performance of the proposed design SCMA codebook compared to the codebooks used for the simulation and results.

6.4 Summary

This chapters uses the Dual Star 16-QAM mother constellation to design a different SCMA codebook. Like the earlier chapter optimization techniques are implemented to increase the MED of the overall mother constellations and partitioning into sub-constellations. The numerical results are then discussed, and shows are superior SCMA codebook design compared to earlier SCMA codebooks designed.

Chapter 7 APSK 4+12 STAR 16-QAM CONSTELLATION PARTITIONING BASED SCMA CODEBOOK

7.1 Introduction

This chapter presents the amplitude phase shift keying (APSK) modulation application for SCMA codebook design. The APSK modulation is the corner stone to all QAM modulation schemes, as QAM employs amplitude variations and phase variations. The modulation scheme has found favour among researchers and industry such as digital broadcasting for satellites (DVB-S2). It is important to note the importance of the selection made as satellites have limitations in power and providing reliable communication. Thus, in this chapter the optimization method incorporates the optimum *RR* principle presented in (Chayratsami & Thuaykaew, 2014). Hence, the effect of *RR* on system performance, such as the BER and PAPR is considered in this Chapter.

7.2 APSK SCMA Codebook Design

The combined modulation technology of amplitude shift keying (ASK) and phase shift keying (PSK) is efficient at utilising the signal space. Thus, improving spectral efficiency of communication systems.

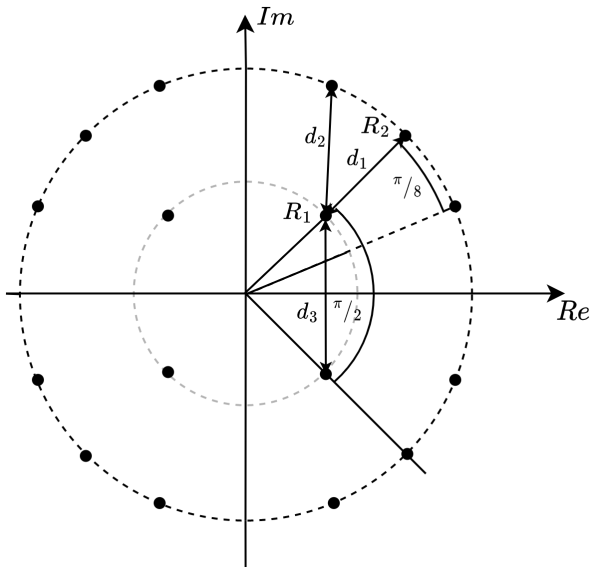

Figure 7.1: APSK Star 16-QAM Mother Constellation

The mother constellation in Figure 7.1 is given by:

$$\mathbf{A}'_{MC} = \begin{cases} \left[R_1 \cos\left(\frac{k\pi}{8}\right), R_1 \sin\left(\frac{k\pi}{8}\right) \right], & k \in \{1,3,5,7\}, \\ \left[R_2 \cos\left(\frac{k\pi}{8}\right), R_2 \sin\left(\frac{k\pi}{8}\right) \right], & k \in \{1,2,3,5,6,7,9,10,11,13,14,15\}, \end{cases}.$$

Optimization of the constellation in Figure 7.1 is performed by optimizing the ring ratio (RR) defined by (6.1) and (6.2).

A single optimal ring ratio for the mother constellation does not exist as shown in Figure 7.2. However, the larger of the two solutions were chosen as the $RR_{\text{opt}} = 2.4142$.

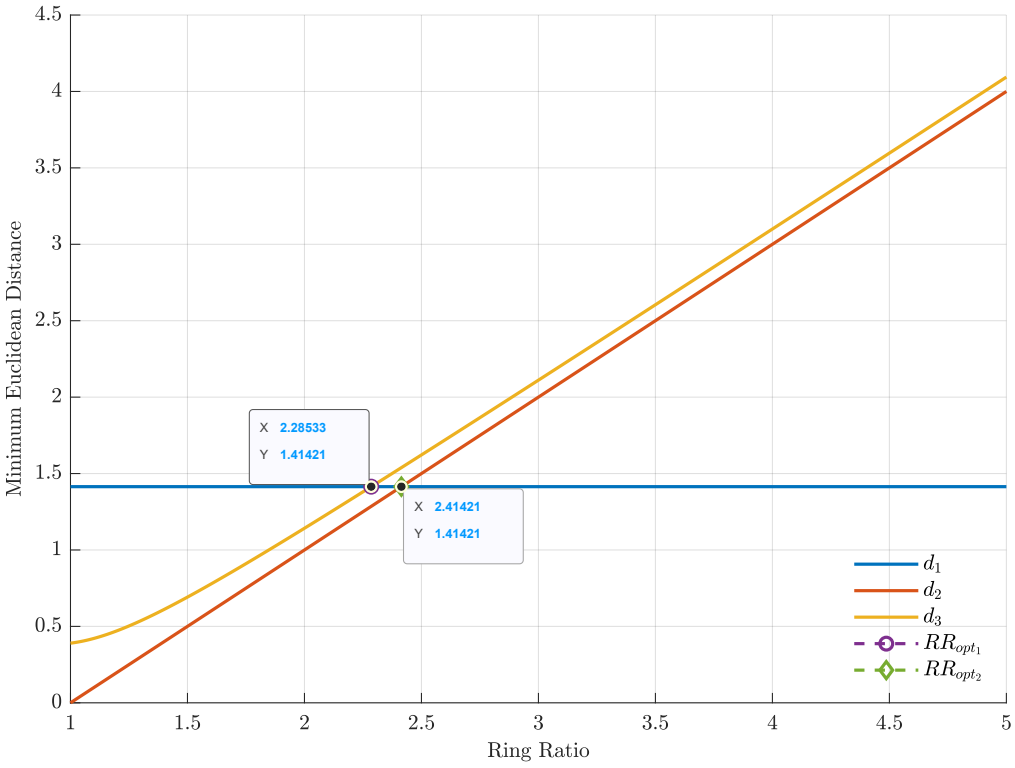

Figure 7.2: Ring Ratio Optimization View of Dual Solution

The partitioning of the mother constellation follows the two-step procedure in Chapter 6, where partitioning is employed and meets the conditions of (4.3).

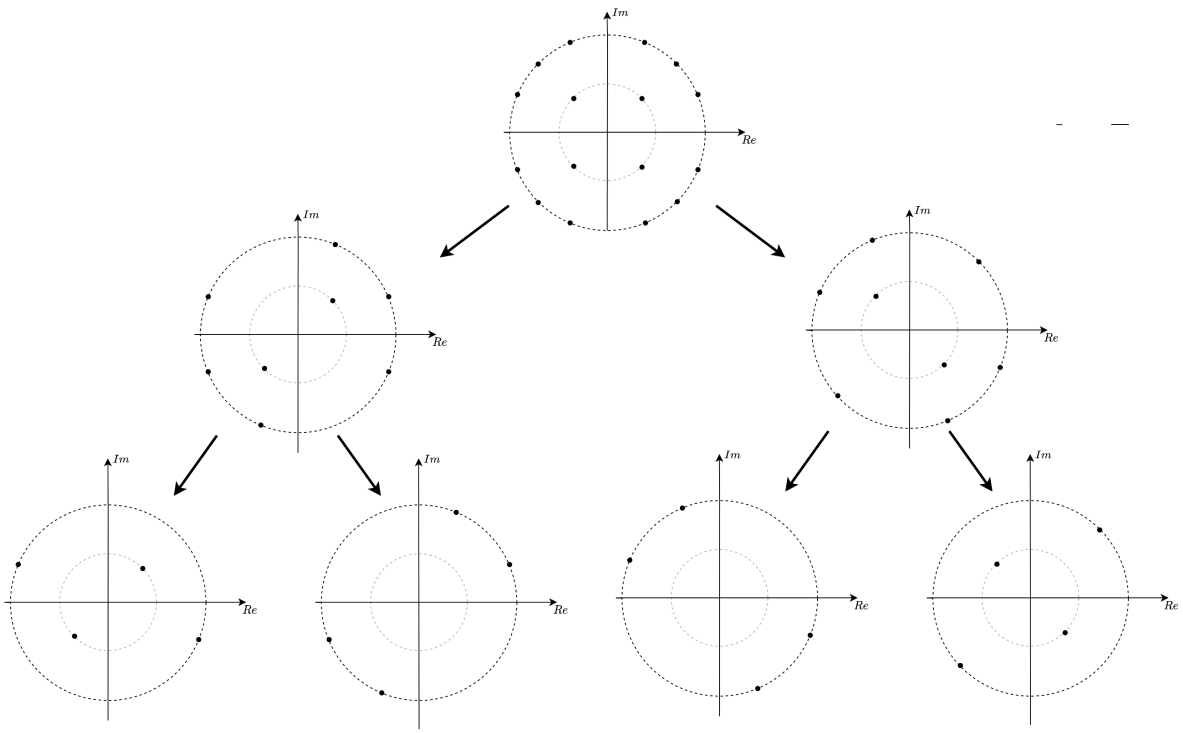

Figure 7.3: APSK Star 16-QAM Mother Constellation

By applying random permutation to the sub-constellations from (5.5) and (3.3) the sub-constellations are randomly allocated to resource elements. Shown in Table 7-1 is one of several possible results due to random permutation of the sub-constellations.

It should be noted that in this instance the signature matrix used in this design has been altered as shown below:

$$\mathbf{F} = \begin{bmatrix} 1 & 0 & 1 & 1 & 0 & 0 \\ 0 & 1 & 0 & 1 & 1 & 0 \\ 1 & 0 & 0 & 0 & 1 & 1 \\ 0 & 1 & 1 & 0 & 0 & 1 \end{bmatrix}$$

Table 7-1 Permutation and Signature Matrix Output

	UE1	**UE2**	**UE3**	**UE4**	**UE5**	**UE6**
RE1	C1	0	C3	C4	0	0
RE2	0	C1	0	C3	C4	0
RE3	C2	0	0	0	C3	C4
RE4	0	C2	C4	0	0	C3

7.2.1 Analysis of the proposed partitioned Dual Star 16-QAM SCMA Constellation

The average signal energy (E) for the system model is fixed at 8.8 and used in conjunction with the RR_{opt} to find the amplitude of R_1 and R_2. The average signal energy is usually defined as:

R_1

$$E = \frac{1}{M}\sum_{i=1}^{M}\|x_i\|^2 . \tag{7.1}$$

Thus, the average signal energy is given by:

$$\begin{aligned} E &= \frac{1}{16}\left(4R_1^2 + 12R_2^2\right) \\ &= \frac{1}{16}\left(4R_1^2 + 12R_1^2 RR_{\text{opt}}\right) \end{aligned} . \tag{7.2}$$

Making R_1 the subject of (5.10) :

$$\begin{aligned} R_1 &= \sqrt{\frac{16E}{4+12RR_{\text{opt}}}} \\ &= \sqrt{\frac{16\cdot 8.8}{8+8\cdot 2.4142}} \\ &= 1.3799 \end{aligned} .$$

R_2 is found by the product of R_1 and RR_{opt} and found to be 3.3315. The larger MED of the conventional 16-QAM constellation, made it an ideal mother constellation candidate. The optimal ring ratio was found to be 1.5867, which resulted in the larger minimum Euclidean distance between neighbouring constellation points of sub-constellations in Table 5-2:

Table 7-2: Partitioning Increases MED of sub-constellations

$\mathbf{A}'_{MC}$	C_1	C_2	C_3	C_4
1.2999	2.7599	2.7599	4.7114	4.7114

Table 7-3 shows the resultant SCMA codebook for the chosen mother constellation with average signal energy fixed at 8.8.

Table 7-3: APSK 4+12 Star 16-QAM SCMA Codebook

USER	USER CODEBOOKS
1	$\begin{bmatrix} 2.3697 + 2.3697i & -0.8680 + 0.8680i & -2.3697 - 2.3697i & 0.8680 - 0.8680i \\ 0.0000 + 0.0000i & 0.0000 + 0.0000i & 0.0000 + 0.0000i & 0.0000 + 0.0000i \\ 0.8680 + 0.8680i & -2.3697 + 2.3697i & -0.8680 - 0.8680i & 2.3697 - 2.3697i \\ 0.0000 + 0.0000i & 0.0000 + 0.0000i & 0.0000 + 0.0000i & 0.0000 + 0.0000i \end{bmatrix}$
2	$\begin{bmatrix} 0.0000 + 0.0000i & 0.0000 + 0.0000i & 0.0000 + 0.0000i & 0.0000 + 0.0000i \\ 2.3697 + 2.3697i & -0.8680 + 0.8680i & -2.3697 - 2.3697i & 0.8680 - 0.8680i \\ 0.0000 + 0.0000i & 0.0000 + 0.0000i & 0.0000 + 0.0000i & 0.0000 + 0.0000i \\ 0.8680 + 0.8680i & -2.3697 + 2.3697i & -0.8680 - 0.8680i & 2.3697 - 2.3697i \end{bmatrix}$
3	$\begin{bmatrix} 1.2825 + 3.0962i & -3.0962 + 1.2825i & -1.2825 - 3.0962i & 3.0962 - 1.2825i \\ 0.0000 + 0.0000i & 0.0000 + 0.0000i & 0.0000 + 0.0000i & 0.0000 + 0.0000i \\ 0.0000 + 0.0000i & 0.0000 + 0.0000i & 0.0000 + 0.0000i & 0.0000 + 0.0000i \\ 3.0962 + 1.2825i & -1.2825 + 3.0962i & -3.0962 - 1.2825i & 1.2825 - 3.0962i \end{bmatrix}$
4	$\begin{bmatrix} 3.0962 + 1.2825i & -1.2825 + 3.0962i & -3.0962 - 1.2825i & 1.2825 - 3.0962i \\ 1.2825 + 3.0962i & -3.0962 + 1.2825i & -1.2825 - 3.0962i & 3.0962 - 1.2825i \\ 0.0000 + 0.0000i & 0.0000 + 0.0000i & 0.0000 + 0.0000i & 0.0000 + 0.0000i \\ 0.0000 + 0.0000i & 0.0000 + 0.0000i & 0.0000 + 0.0000i & 0.0000 + 0.0000i \end{bmatrix}$
5	$\begin{bmatrix} 0.0000 + 0.0000i & 0.0000 + 0.0000i & 0.0000 + 0.0000i & 0.0000 + 0.0000i \\ 3.0962 + 1.2825i & -1.2825 + 3.0962i & -3.0962 - 1.2825i & 1.2825 - 3.0962i \\ 1.2825 + 3.0962i & -3.0962 + 1.2825i & -1.2825 - 3.0962i & 3.0962 - 1.2825i \\ 0.0000 + 0.0000i & 0.0000 + 0.0000i & 0.0000 + 0.0000i & 0.0000 + 0.0000i \end{bmatrix}$
6	$\begin{bmatrix} 0.0000 + 0.0000i & 0.0000 + 0.0000i & 0.0000 + 0.0000i & 0.0000 + 0.0000i \\ 0.0000 + 0.0000i & 0.0000 + 0.0000i & 0.0000 + 0.0000i & 0.0000 + 0.0000i \\ 3.0962 + 1.2825i & -1.2825 + 3.0962i & -3.0962 - 1.2825i & 1.2825 - 3.0962i \\ 1.2825 + 3.0962i & -3.0962 + 1.2825i & -1.2825 - 3.0962i & 3.0962 - 1.2825i \end{bmatrix}$

7.3 Numerical Simulations and Results Analyses of the proposed APSK SCMA Codebook Design.

As in Chapter 6 the SCMA codebook performance is compared with existing codebook designs in (Liu et al., 2018), and (Nikopour & Baligh, 2013), the undivided 16-QAM SCMA codebook in (Yu et al., 2016) and the trellis coded modulation SCMA subset division based on 16-QAM in (Nikopour & Baligh, 2013). The system parameters in Table 6-4 is based on the model in (Liu et al., 2018), which is used for simulations and results.

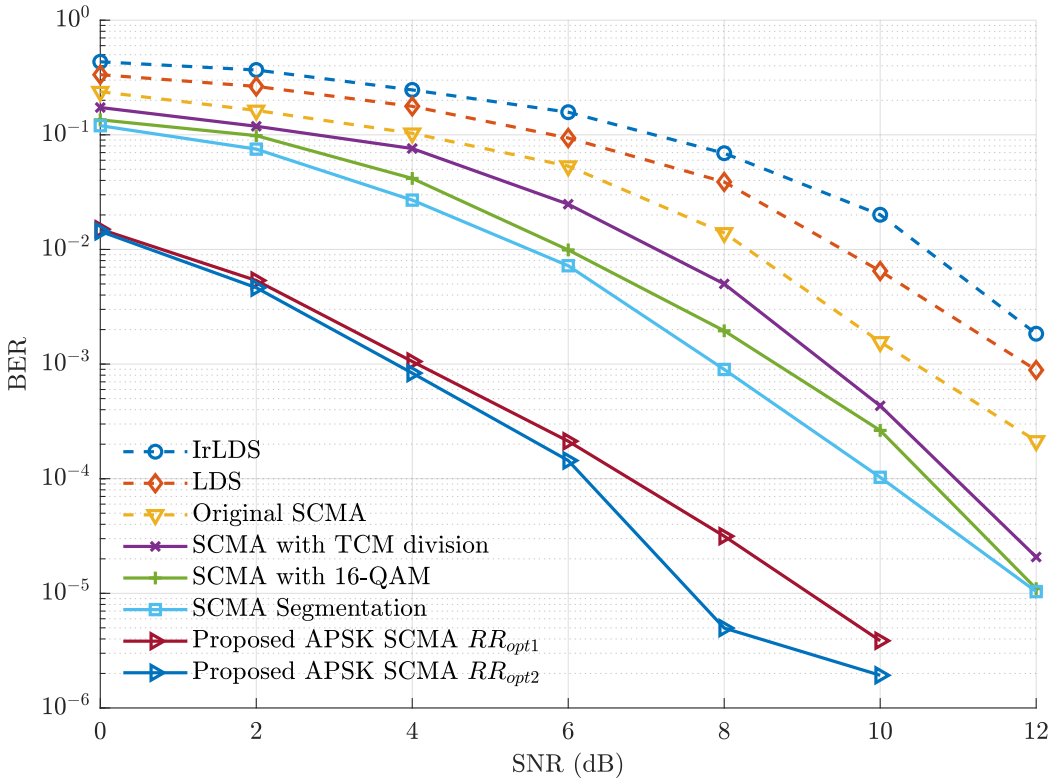

Figure 7.4: BER Performance Comparison between different SCMA Codebooks.

Results in Figure 7.4 show the proposed APSK Star 16-QAM exceeds the existing SCMA codebook designs at low and high SNR. At SNR = 6.21 dB and BER=10^{-4} dB, the proposed SCMA codebook design outperforms the existing designs. Specifically, the proposed codebook design yields a 3.79 dB BER performance gain as compared to the SCMA segmented codebook in (Liu et al., 2018). More so, the proposed Dual Ring Star 16-QAM SCMA codebook design shows considerable performance gain of 4.79 dB, 5.19 dB, 6.29 dB, 7.29 dB and 7.79 dB as compared to (Yu et al., 2015), (Liang et al., 2017), and the LDS and IrLDS schemes in (Cheng et al., 2015) respectively. RR_{opt2} performance is 0.58 dB better than RR_{opt1} at 10^{-4} dB.

The performance increase in BER can be explained by the larger MED of 2.7599, which is achieved by choosing an optimal mother constellation and performing constellation partitioning on the mother constellation. Applying (4.1) the MEDS of authors (Liu et al., 2018), (Yu et al., 2015) and (Liang et al., 2017) are revealed to have the values of 2.11, 1.7654, 1.414 respectively.

Table 7-4 Comparison of MED among different SCMA Codebooks

Codebooks	MED	SNR at BER of 10^{-4} (dB)	BER Gain (dB)
Proposed SCMA Codebook	4	6.21	
Segmented SCMA Codebook	2.11	10	3.79
SCMA with 16-QAM	1.765	11	4.79
SCMA with TCM division	1.414	11.4	5.19
Original SCMA	1	12.5	6.29
LDS	N/A	13.5	7.29
IrLDS	N/A	14	7.79

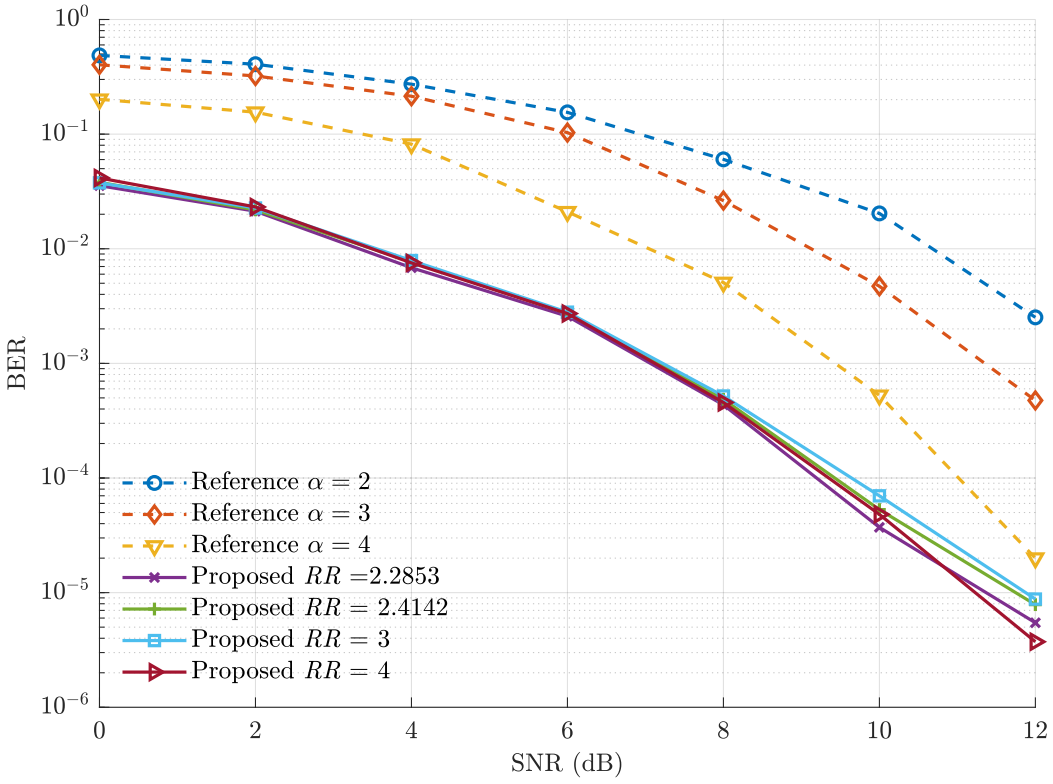

Figure 7.5: Performance Comparison at different RR over a Rayleigh Fading Channel

Reviewing Figure 7.5 the ring ratios of the APSK SCMA codebooks has not changed the overall BER performance. It is notable that at high SNR the *RR*=4 has marginal BER performance gain over the other APSK SCMA codebooks. Due to the larger number of constellation points on the outer ring of the APSK Star 16-QAM. The optimization of the *RR* should have been placed on the outer ring instead of satisfying both inner and outer neighbouring constellation points.

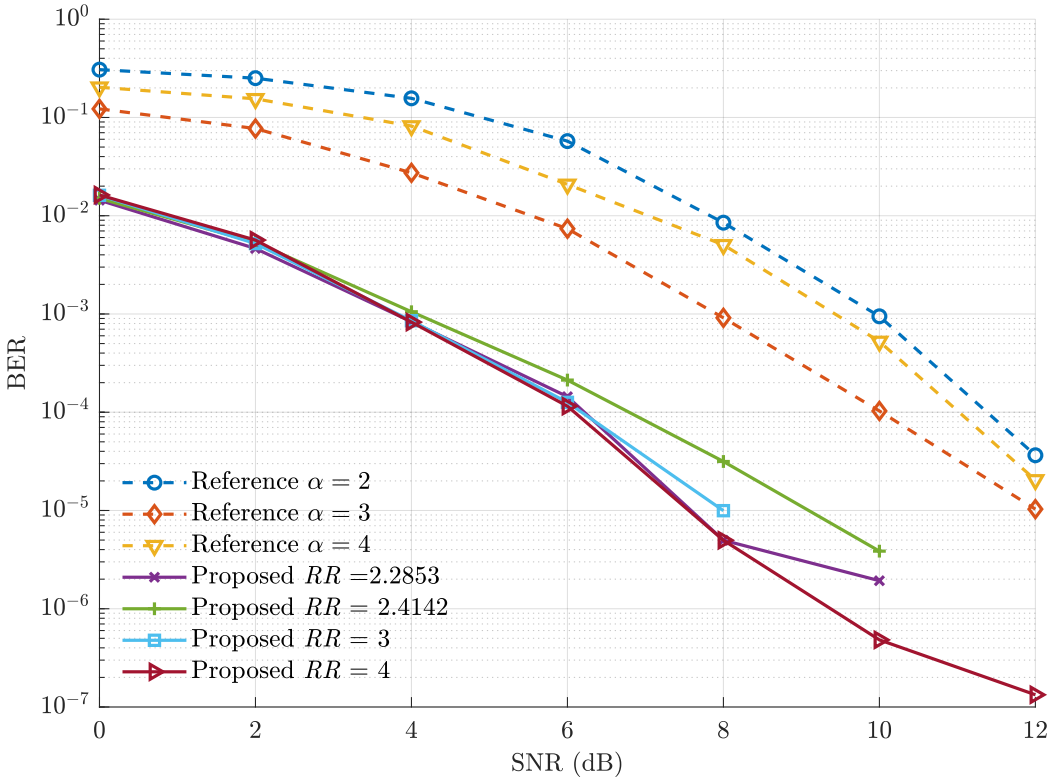

Figure 7.6: Performance Comparison at different RR over a Nakagami-m Fading Channel

Analysis of Figure 7.6 as in the Rayleigh fading channel the larger *RR*=4 surpasses all other APSK SCMA codebooks at higher SNR. The chosen $RR_{opt} = 2.4142$ is surpassed by the larger *RR*=4 by nearly 2 dB at BER = 10^{-5}. The *RR*=2.2853, one of the dual solutions performs well at low SNR and marginally better than RR_{opt}. *RR*=4 is superior to the scheme presented by authors (Liu et al., 2018) by 4.5 dB at BER = 10^{-5}.

7.4 Summary

This chapters uses the 4+12 APSK mother constellation to design a different SCMA codebook. Like Chapter 6 optimization techniques are implemented to increase the MED of the overall mother constellations and partitioning into sub-constellations. The numerical results are then discussed, and shows are superior SCMA codebook design compared to earlier SCMA codebooks designed. Results of the APSK SCMA codebook design are marginally different than theory suggested. This is due to the unique constellation points loading on the inner and outer rings.

8.1 Conclusion

This research introduces the evolution of communication and the demand driving the need for new technologies. The fourth-generation communications system has laboured to meet the ever-increasing demands of consumers. An extensive review on the evolution of technology is presented, with advantages and disadvantages. The paradigm in this research is to address the spectrum limitations and as well as serving multiple devices. An extensive literature review takes a cookbook approach on how to solve spectral limitations and presents the solutions as SCMA codebook design. The contrasting technique uses non-orthogonal multiple access techniques; able to support overloading of user information on resource elements.

Literature further discusses the receiver decoders required to enable overloading resource elements. Thus, highlighting the two the key components of SCMA communication, namely designing effective SCMA codebooks and decoders.

The main contribution of this research is the result of optimizing the minimum Euclidean distance (MED) between neighbouring constellation points of a mother constellation. Then applying the partitioning criterion to further increase the MED. Simulated over varying fading channels on the uplink to a base station. The mother constellations chosen were APSK (4+12) and 16-QAM as these constellations are commonly used throughout the communication system.

The results correlated with the theory stating the increase in MED reduces the probability of error. Thus, increased the BER performance over the communication system model due to lowered collisions of user information.

It should be noted that the APSK Star 16-QAM reacted differently, by outperforming the optimal ring ratio calculated according to theory. However, this might have been due the APSK constellations being a 4+12 APSK mother constellation. Where most of the constellations were on the outer ring and not balanced as the Conventional Star 16-QAM and the Dual Star 16-QAM.

8.2 Future Work

Analysis of the user information showed interesting results considering individual user performances. There were instances where approximately half of users demonstrated improved BER performance over others.

I would like to take this further and implement SCMA and power allocation techniques to further improve the results I have seen. The power allocation is also a NOMA technique and allocates power according to the user channel conditions. Users with the worst channel conditions are then allocated more power than those with better channel conditions.

I believe this two-fold technique would really improve the uplink and downlink performance and could bring us closer to realizing the drivers set for 5G technology.

BIBLIOGRAPHY

Aldababsa, M., Toka, M., Gökçeli, S., Kurt, G.K. & Kucur, O. 2018. A Tutorial on Nonorthogonal Multiple Access for 5G and Beyond. *Wireless Communications and Mobile Computing*, 2018: 1–24.

Ameur, W. Ben, Mary, P., Dumay, M., Hélard, J., Schwoerer, J., Helard, J.F. & Schwoerer, J. 2019. Performance study of mpa, log-mpa and max-log-mpa for an uplink scma scenario. *2019 26th International Conference on Telecommunications, ICT 2019*: 411–416.

Balyan, V. & Daniels, R. 2020. Resource allocation for NOMA based networks using relays: cell centre and cell edge users. *International Journal on Smart Sensing and Intelligent Systems*, 13(1): 1–18.

Press, R & Balyan, V.2022. Outage probability for a multiuser NOMA-based network using energy harvesting relays. *Nonlinear Engineering*, vol. 11, no. 1, 2022, pp. 672-679. https://doi.org/10.1515/nleng-2022-0240

Binh, L.N. 2017. *Optical Modulation*. L. N. Binh, ed. CRC Press.

Cai, D., Fan, P., Lei, X., Liu, Y. & Chen, D. 2016. Multi-Dimensional SCMA Codebook Design Based on Constellation Rotation and Interleaving. In *2016 IEEE 83rd Vehicular Technology Conference (VTC Spring)*. IEEE: 1–5.

Chandrasetty, V.A. & Aziz, S.M. 2009. A reduced complexity message passing algorithm with improved performance for LDPC decoding. *ICCIT 2009 - Proceedings of 2009 12th International Conference on Computer and Information Technology*, (January): 19–24.

Chaturvedi, S., Liu, Z., Bohara, V.A., Srivastava, A. & Xiao, P. 2022. A Tutorial on Decoding Techniques of Sparse Code Multiple Access. *IEEE Access*, 10: 58503–58524.

Chaturvedi, S., Liu, Z., Bohara, V.A., Srivastava, A. & Xiao, P. 2021. A Tutorial to Sparse Code Multiple Access. : 1–14.

Chayratsami, P. & Thuaykaew, S. 2014. The optimum ring ratio of 16-APSK in LTE uplink over nonlinear system. *International Conference on Advanced Communication Technology, ICACT*: 322–328.

Chege, S. & Walingo, T. 2022. MIMO hybrid PD-SCMA NOMA Uplink Transceiver System. *IEEE Access*, 10(July): 88138–88151.

Chen, C., Tian, H. & Nie, G. 2020. Fairness Resource Allocation Scheme for GBR Services in Downlink SCMA System. *2020 IEEE/CIC International Conference on Communications in China, ICCC 2020*, (Iccc): 190–195.

Cheng, M., Wu, Y. & Chen, Y. 2015. Capacity analysis for non-orthogonal overloading transmissions under constellation constraints. *2015 International Conference on Wireless Communications and Signal Processing, WCSP 2015*.

Cover, T.M. & Thomas, J.A. 1991. Information theory and the stock market. *Elements of Information Theory. Wiley Inc., New York*: 543–556.

Dai, L., Wang, B., Ding, Z., Wang, Z., Chen, S. & Hanzo, L. 2018. A survey of non-orthogonal multiple access for 5G. *IEEE Communications Surveys and Tutorials*, 20(3): 2294–2323.

Dai, L., Wang, B., Yuan, Y., Han, S., I, C.L. & Wang, Z. 2015. Non-orthogonal multiple access for 5G: Solutions, challenges, opportunities, and future research trends. *IEEE Communications Magazine*, 53(9): 74–81.

Dangi, R., Lalwani, P., Choudhary, G. & You, I. 2022. Study and Investigation on 5G Technology : A Systematic Review. : 1–32.

David Falconer. 2011. *Error Control and Adaptation in Digital Communication Networks*. Cambridge University Press.

Deka, K., Priyadarsini, M., Sharma, S. & Beferull-Lozano, B. 2020. Design of SCMA codebooks using differential evolution. *2020 IEEE International Conference on Communications Workshops, ICC Workshops 2020 - Proceedings*.

Deka, K. & Sharma, S. 2022. Hybrid NOMA for Future Radio Access: Design, Potentials and Limitations. *Wireless Personal Communications*, 123(4): 3755–3770. https://doi.org/10.1007/s11277-021-09312-3.

Fossorier, M.P.C., Mihaljevic, M. & Imai, H. 1999. Reduced complexity iterative decoding of low-density parity check codes based on belief propagation. *IEEE Transactions on communications*, 47(5): 673–680.

Ghaffari, A., Leonardon, M., Cassagne, A., Leroux, C. & Savaria, Y. 2019. Toward high-performance implementation of 5G SCMA algorithms. *IEEE Access*, 7: 10402–10414.

Ghafoor, U., Ali, M., Zubair, H. & Masood, A. 2022. Journal of Network and Computer Applications NOMA and future 5G & B5G wireless networks : A paradigm. *Journal of Network and Computer Applications*, 204(December 2021): 103413. https://doi.org/10.1016/j.jnca.2022.103413.

Hagenauer, J. 1988. Rate-compatible punctured convolutional codes (RCPC codes) and their applications. *IEEE Transactions on Communications*, 36(4): 389–400.

Haykin, S. 2008. *Communication systems*. John Wiley & Sons.

Hernandez, D.L., Proano, E.O., Mora, H.C., Garzon, N.O. & Frison, C.I. 2020. Bit error rate evaluation of SCMA in rician fading channels considering presence of co-cell interference. *2020 Ieee Andescon, Andescon 2020*: 6–11.

Hidayat, I., Meylani, L., Kurniawan, A., Arifianto, M.S. & Anwar, K. 2021. Investigating Mother Constellation of SCMA Systems Having Capability of Multiuser Detection. *Proceedings of the 2021 IEEE Symposium on Future Telecommunication Technologies, SOFTT 2021*, (10): 52–56.

Huang, C., Su, B., Lin, T. & Huang, Y. 2022. Downlink SCMA Codebook Design with Low Error Rate by Maximizing Minimum Euclidean Distance of Superimposed Codewords. *IEEE Transactions on Vehicular Technology*, 71(5): 5231–5245. https://ieeexplore.ieee.org/document/9727076/.

Jehan, A., Zeeshan, M. & Ashraf, T. 2021. Parametric Analysis of SCMA Performance with Different Codebooks and Orthogonal Resources. *2021 International Conference on Robotics and Automation in Industry, ICRAI 2021*: 3–7.

Khanh, Q.V., Hoai, N.V., Manh, L.D., Le, A.N. & Jeon, G. 2022. Wireless Communication Technologies for IoT in 5G: Vision, Applications, and Challenges. *Wireless Communications and Mobile Computing*, 2022.

Kiraci, F., Bardakci, E., Sadi, Y. & Erkucuk, S. 2020. The Effect of Codebook Design on the Conventional SCMA System Performance. *2020 28th Signal Processing and Communications Applications Conference, SIU 2020 - Proceedings*: 2020–2023.

Knill, O. 2023. Probability Theory and Stochastic Processes with Applications. *Probability Theory and Stochastic Processes with Applications*.

Kschischang, F.R., Frey, B.J. & Loeliger, H.A. 2001. Factor graphs and the sum-product algorithm. *IEEE Transactions on Information Theory*, 47(2): 498–519.

Kumagai, Y., Gonda, N., Shimbo, Y., Suganuma, H. & Maehara, F. 2021. Deep Learning Based Hybrid Multiple Access Consisting of SCMA and OFDMA Using User Position Information. *3rd International Conference on Artificial Intelligence in Information and Communication, ICAIIC 2021*: 10–13.

Lei, T.F., Zhang, A. di, ShuYan, N., Song, X., Cheng, N.P. & Yan, D.S. 2021. SCMA-OFDM Codebook Design based on IRM. *2021 International Wireless Communications and Mobile Computing, IWCMC 2021*: 735–739.

Liang, Y., Yu.B & Tong, K, M. 2017. Simple SCMA Codebook design in AWGN channels. http://www.arocmag.com/article/02-2017-09-001.html.

Liu, P., An, K., Lei, J., Zheng, G., Sun, Y. & Liu, W. 2022. SCMA-Based Multiaccess Edge Computing in IoT Systems: An Energy-Efficiency and Latency Tradeoff. *IEEE Internet of Things Journal*, 9(7): 4849–4862.

Liu, S., Wang, J., Bao, J. & Liu, C. 2018. Optimized SCMA Codebook Design by QAM Constellation Segmentation With Maximized MED. *IEEE Access*, 6: 63232–63242.

Liu, Z. & Yang, L.L. 2021. Sparse or Dense: A Comparative Study of Code-Domain NOMA Systems. *IEEE Transactions on Wireless Communications*, 20(8): 4768–4780.

Mardinata, V.A., Kurniawan, D. & Armi, N. 2021. Impact of Overloading Factor on MIMO-SCMA Systems. *Proceeding - 2021 International Conference on Radar, Antenna, Microwave, Electronics, and Telecommunications: Managing the Impact of Covid-19 Pandemic: Together Facing Challenges Through Electronics and ICTs, ICRAMET 2021*: 95–98.

Mheich, Z., Wen, L., Xiao, P. & Maaref, A. 2019. Design of SCMA Codebooks Based on Golden Angle Modulation. , 68(2): 1501–1509.

Mou, S., Dai, J. & Si, Z. 2020. Extended SCMA Graphs for Block Fading Channels. *2020 IEEE/CIC International Conference on Communications in China, ICCC 2020*, (Iccc): 929–934.

Nikopour, H. & Baligh, H. 2013. Sparse code multiple access. In *2013 IEEE 24th Annual International Symposium on Personal, Indoor, and Mobile Radio Communications (PIMRC)*. IEEE: 332–336.

Pana, Vuyo S, Babalola, O.P. & Balyan, V. 2022. 5G radio access networks: A survey. *Array*: 100170.

Pana, Vuyo S., Balyan, V. & Groenewald B, 2020. Machine-to-machine and cell-to-cell traffic handling using relay and carrier aggregation prioritize on LTE-A PRO network, *International Journal on Smart Sensing and Intelligent*

Proakis, J.G. & Salehi, M. 2007. Digital Communications, 5th expanded ed.

Rappaport, T.S. 2002. *Wireless Communications: Principles and Practice*. 1st ed. T. S. Rappaport, ed. Michigan: Prentice Hall PTR.

Rice, M. 2009. *Digital communications: a discrete-time approach*. Pearson Education India.

Robertson, P., Villebrun, E. & Hoeher, P. 1995. A comparison of optimal and sub-optimal MAP decoding algorithms operating in the log domain. In *Proceedings IEEE International Conference on Communications ICC'95*. IEEE: 1009–1013.

Shah, B.M., Murtaza, M. & Raza, M. 2020. Comparison of 4G and 5G Cellular Network Architecture and Proposing of 6G, a new era of AI. *CITISIA 2020 - IEEE Conference on Innovative Technologies in Intelligent Systems and Industrial Applications, Proceedings*.

Sklar Bernard. 2016. *Digital Communications: Fundamentals and Applications*. 2nd ed. Prentice Hall.

Suyama, S., Okuyama, T., Nonaka, N. & Asai, T. 2022. Recent Studies on Massive MIMO Technologies for 5G Evolution and 6G. : 3–6.

Taherzadeh, M., Nikopour, H., Bayesteh, A. & Baligh, H. 2014. SCMA codebook design. *IEEE Vehicular Technology Conference*: 1–5.

Tranter, W.H., Shanmugan, K.S., Rappaport, T.S. & Kosbar, K.L. 2003. *of Communication Systems Simulation with Wireless Applications*.

Vaezi, M., Ding, Z. & Vincent Poor, H. 2018. *Multiple access techniques for 5G wireless networks and beyond*.

Vidal-Beltrán, S. & López-Bonilla, J.L. 2021. Improving Spectral Efficiency in the SCMA Uplink Channel. *Mathematics*, 9(6): 651.

Vikas, V., Rajesh, A., Deka, K. & Sharma, S. 2022. A Comprehensive Technique to Design SCMA Codebooks. *IEEE Communications Letters*, 7798(c): 1–5.

Wang, S., Lai, K., Lei, J. & Wen, L. 2021. Low PAPR SCMA systems based on carrier techniques. *2021 IEEE/CIC International Conference on Communications in China, ICCC 2021*, (Iccc): 370–375.

Yan, C., Kang, G. & Zhang, N. 2017. A Dimension Distance-Based SCMA Codebook Design. *IEEE Access*, 5: 5471–5479.

Yang, P., Xiao, Y., Zhang, B., Li, S., El-Hajjar, M. & Hanzo, L. 2014. Star-QAM signaling constellations for spatial modulation. *IEEE Transactions on Vehicular Technology*, 63(8): 3741–3749.

Yu, L., Fan, P., Ma, Z., Lei, X. & Chen, D. 2016. An optimized design of irregular SCMA codebook based on rotated angles and EXIT chart. *IEEE Vehicular Technology Conference*, 0.aa

Yu, L., Lei, X., Fan, P. & Chen, D. 2015. An optimized design of SCMA codebook based on star-QAM signaling constellations. *2015 International Conference on Wireless Communications and Signal Processing, WCSP 2015*: 1–5.aa

Zhang, L.M. & Kschischang, F.R. 2017. Low-complexity soft-decision concatenated LDGM-staircase FEC for high-bit-rate fiber-optic communication. *Journal of Lightwave Technology*, 35(18): 3991–3999.

a